The Cryosphere Discuss., https://doi.org/10.5194/tc-2019-44
Manuscript under review for journal The Cryosphere
Discussion started: 21 March 2019

The Cryosphere Discussions
Open Access
EGU

Impact of floe size distribution on seasonal fragmentation and melt of Arctic sea ice

Adam W. Bateson[1], Daniel L. Feltham[1], David Schröder[1], Lucia Hosekova[1], Jeff K. Ridley[2], Yevgeny Aksenov[3]

[1]Department of Meteorology, University of Reading, Reading, RG2 7PS, United Kingdom
[2]Hadley Centre for Climate Prediction and Research, Met Office, Exeter, EX1 3PB, United Kingdom
[3]National Oceanography Centre Southampton, Southampton, SO14 3ZH, United Kingdom

Correspondence to: Adam W. Bateson (a.w.bateson@pgr.reading.ac.uk)

Abstract. Recent years have seen a rapid reduction in the summer Arctic sea ice extent. To both understand this trend and project the future evolution of the summer Arctic sea ice, a better understanding of the physical processes that drive the seasonal loss of sea ice is required. The marginal ice zone, here defined as regions with between 15 and 80% sea ice cover, is the region separating pack ice from open ocean. Accurate modelling of this region is important to understand the dominant mechanisms involved in seasonal sea ice loss. Evolution of the marginal ice zone is determined by complex interactions between the atmosphere, sea ice, ocean, and ocean surface waves. Therefore, this region presents a significant modelling challenge. Sea ice floes span a range of sizes but climate sea ice models assume they adopt a constant size. Floe size influences the lateral melt rate of sea ice and momentum transfer between atmosphere, sea ice, and ocean, all important processes within the marginal ice zone. In this study, the floe size distribution is represented as a truncated power law defined by three key parameters: minimum floe size, maximum floe size, and power law exponent. This distribution is implemented within a sea ice model coupled to a prognostic ocean mixed layer model. We present results to show that the use of a power law derived floe size distribution has a spatially and temporally dependent impact on the sea ice, in particular increasing the role of the marginal ice zone in seasonal sea ice loss. This feature is important in correcting existing biases within sea ice models. In addition, we show a much stronger model sensitivity to floe size distribution parameters than other parameters used to calculate lateral melt, justifying the focus on floe size distribution in model development. It is finally concluded that the model approach presented here is a flexible tool for assessing the importance of a floe size distribution in the evolution of sea ice and is suitable for applications where a simple but realistic floe size distribution model is required.

1 Introduction

Arctic sea ice is an important component of the climate system. The sea ice cover moderates high latitude energy transfers between the ocean and atmosphere (Screen et al., 2013) and generates a positive feedback response to global warming via the albedo feedback mechanism (Dickinson et al., 1987; Winton, 2006, 2013). Accurate representation of the sea ice within climate models can contribute to improved projections of the climate response to present and future forcings (Vihma, 2014). On a more local scale sea ice modelling is necessary to understand how environments within and around the Arctic are likely to develop. This is important for Arctic communities to plan for the future (Laidler et al., 2009), to enable ecologists to identify practical responses to protect vulnerable species that live in the Arctic or seasonally migrate into the region (Hauser et al., 2017; Post et al., 2009; Regehr et al., 2010), and shipping companies to understand the potential viability of new routes in the next few decades (Aksenov et al., 2017; Ho, 2010; Smith and Stephenson, 2013).

The Arctic is currently in a state of transition (Notz and Stroeve, 2018; Stroeve and Notz, 2018). Multiyear ice fraction has decreased by more than 50% with an increasing proportion of the ice cover now seasonal first year ice (Kwok, 2018; Maslanik et al., 2007). First year ice does not have the same surface roughness or the same mechanical or thermophysical (salinity, conductivity, permeability) properties as ice that has developed over multiple years. In particular, first year ice is thinner and

weaker (Stroeve et al., 2018) and hence more vulnerable to fracture in response to external stress (Zhang et al., 2012). Similarly the region of the Arctic described as marginal, defined here as where the ice area fraction extends between 15 and 80%, is projected to increase in extent (Aksenov et al., 2017).

Modelling the Marginal Ice Zone (MIZ) is a significant challenge due to its complexity; it is a region in which there is strong coupling between the sea ice, ocean and atmosphere (Lee et al., 2012; McPhee et al., 1987). The proximity of the MIZ to the open ocean and incomplete ice coverage means these are regions into which ocean waves can propagate and fracture the ice cover (Liu et al., 1992). Wave intensity and storm frequency are projected to increase, which will strengthen wave-ice interactions (Sepp and Jaagus, 2011). This continues a trend already observed over the past few decades (Stopa et al., 2016). Such interactions are even more prominent around Antarctica due to the dominance of seasonal sea ice in the region (Parkinson and Cavalieri, 2012) and large and increasing wave fetch (Young et al., 2011).

Floe size is a key parameter in describing the evolution of the MIZ (Rothrock and Thorndike, 1984). As sea ice floes become smaller the available perimeter per unit area of sea ice cover increases, enhancing the lateral melt rate (Steele, 1992). Increased lateral ice melt increases the area of exposed ocean, allowing the input of more heat into the ocean mixed layer from solar insolation. Warming of the upper mixed layer also re-stratifies the ocean. These two processes increase heat available for ice melt through basal and lateral ice melting mechanisms. The former is a well-known mechanism, the albedo feedback (Curry et al., 1995). As more of the ice becomes marginal, the lateral ice melting is expected to become an increasingly significant driver of seasonal ice loss.

Currently climate models either assume a fixed and constant characteristic floe size (calliper) across the Arctic cover, for all types of sea ice (Hunke et al., 2015), or they ignore floe size entirely. This assumption both simplifies the model code and reduces computational costs of running the model. However, this approach does not allow for regional or temporal variations in floe size. Multiple sea ice processes depend on floe size. Lateral melt rate is a function of floe size; the melt rate is proportional to the perimeter per unit area of sea ice. A recent study has found that the basal melt rate may also be influenced by floe size (Horvat and Tziperman, 2018). Floe size can also impact the propagation of waves under the ice (Boutin et al., 2018; Meylan and Squire, 1994; Squire, 2007). The assumption of a fixed floe size also precludes sea ice models from accurately representing the role of processes within sea ice evolution that can change floe size such as lateral melting and wave induced fragmentation of floes. Whilst these assumptions are significant, the use of a variable floe size within models will need to be justified against the increased computational cost. Context dictates the most suitable approach; higher complexity floe size representation will be required for high resolution regional sea ice modelling than for large scale climate models.

There have been several observational studies aiming to characterise the floe size distribution (FSD) using techniques including satellite imagery and in-situ studies (Stern et al., 2018a). FSD data is generally fitted to a truncated power law (Rothrock and Thorndike, 1984). Values have been reported for the exponent of this power law ranging from -1.5 to below -3.5 between different datasets (Stern et al., 2018a). Comparing these observations is complicated by the fact that some studies report a value for the probability distribution of floe size, and some for the cumulative floe size distribution. It has been recently pointed out that if a distribution adopts a truncated power law for a probability distribution, it will have a tailing off for larger floes when plotted as a cumulative distribution (Stern et al., 2018a). Furthermore, a recent study (Stern et al., 2018b) found evidence to suggest that the exponent of the power law FSD evolves throughout the year and is not fixed. This same study was also able to use two satellite data sets with different resolutions but operating over the same region to show a consistent power law over floes from as small as 10 m and as large as 30,000 m. Other studies find different values for these limits, for example Toyota et al. (2016) showed a power law extending to 1 m (using data collected *in situ* from a ship), whereas Hwang et al. (2017) found a tailing off from the power law around 300 – 400 m. As each study operates over a different spatial extent, with a different resolution and different algorithms used to extract the FSD, it is not trivial to identify whether the cut-offs in each scenario are physical or a product of limited resolution or spatial extent. Alternative approaches to a single power law have been proposed including the use of two power laws over different size ranges, with smaller floes found to have a smaller

exponent (Steer et al., 2008). The Pareto distribution has also been discussed (Herman, 2010); it is analogous to a power law but with a non-constant exponent. To fully understand and characterise the FSD across the Arctic sea ice good spatial and temporal coverage is required. Novel techniques, particularly those using autonomous platforms and robotic instruments, are enabling increased high-resolution data capture (Thomson and Lee, 2017); the collection and output of this data remains in progress. There are also efforts to characterise the floe size distribution resulting from individual processes, such as laboratory analogues to the wave breakup of ice (Herman et al., 2018). Future Arctic expeditions including "Multidisciplinary drifting Observatory for the Study of Arctic Climate" (MOSAiC, Dethloff et al., 2016), planned to last one year within the central Arctic, should contribute to the existing FSD datasets.

Modelling studies have used contrasting approaches to represent floes as a distribution. A very simple approach is the use of a semi-empirical relationship between floe size and ice concentration (Lüpkes et al., 2012; Tsamados et al., 2015). Although this approach involves a simple amendment to the code and has a negligible computational cost, it is unable to respond to fragmentation processes. It will not capture the desired feedbacks during events such as storms that are expected to produce significant fragmentation of the sea ice cover. Furthermore, the parameters used within the relationship were constrained by a set of observations from a specific region and season and might not be applicable across the whole sea ice fraction and full seasonal cycle.

Extending beyond using this simple dependency of floe size on ice concentration, Zhang et al. (2015) introduced a thickness, floe size and enthalpy distribution. This model aims to represent the impacts on floe size of advection, thermodynamic growth, lateral melting, ice ridging and ice fragmentation. However, the impacts of wind, current and wave forcing are represented by an empirically parameterised floe size distribution factor. Bennetts et al. (2017) focus on the incorporation of a physically realistic wave-induced break up model (Williams et al., 2013a, 2013b). Bennetts et al. (2017) assume that the FSD follows a split power law, with a change in exponent at some critical diameter. The wave component of this model assumes steady-state conditions over a timestep and uses a Bretschneider spectrum defined by a significant wave height and a peak period for computational efficiency and propagates it in the mean wave direction. The propagation directions are calculated from averages of the wave directions entering the neighbouring cells and weighted according to the respective wave energy. The model implementation also assumes floe sizes to be assigned to a minimum representative diameter if ice is too thin and compliant to be broken by waves.

There has also been a significant drive to develop a physically derived prognostic floe size-thickness distribution (Horvat and Tziperman, 2015, 2017; Roach et al., 2018a). A recent approach by Roach et al. (2018a) includes the representation of five processes: new ice formation; welding of floes; lateral growth; lateral melt; and fracture by ocean surface waves. This model has the advantage that it does not involve any assumptions about the form of the distribution. Provided the model incorporates good physical representations of the processes which impact floe size, the model should respond accurately to localised extremes in behaviour (such as the large waves associated with storms), or future changes (e.g. changing wind speeds). It is also possible to model floe evolution at the floe by floe scale, for example Herman (2018) uses a discrete-element model to investigate the wave-induced behaviour of floes. However, these are computationally expensive approaches. This may be acceptable for use within a standalone sea ice model but coupled-climate modellers will be reluctant to accept a significant cost without evidence that it has a significant impact on how the sea ice interacts with the climate system.

For this study, a single truncated power law will be applied to describe the FSD within a standalone sea ice model coupled to a prognostic mixed layer model, hereafter referred to as the WIPoFSD model (Waves-in-Ice module and Power law Floe Size Distribution model). The distribution is defined by three parameters: minimum floe size; maximum floe size and the exponent. The exponent and minimum floe size are set to fixed values. However, the maximum floe size evolves between fixed limits in response to four key processes: wave induced break-up; lateral melting; advection; and a restoring mechanism in freezing conditions. The WIPoFSD model has been selected as it is able to respond to processes that influence floe size without the computational expense of a full prognostic FSD model. The model allows an assessment of how a power law distribution of

floes will impact the ice cover and by what mechanisms these changes occur. Furthermore, it provides a simple framework to explore the model sensitivity to the three parameters used to define the WIPoFSD. This framework also lends itself to a series of additional experiments including imposing a variable exponent, changing the parameters that define the impact of waves on sea ice, and comparing the model sensitivity of the floe size parameters to other parameters that influence the lateral melt rate. A standalone sea ice model has been selected over a coupled approach to limit model complexity so that the physical impacts and feedbacks of imposing the WIPoFSD model can be more easily identified and to allow time for more sensitivity studies. This is coupled to a prognostic mixed layer so that mixed layer feedbacks can also be considered.

This paper will proceed as follows. Section 2 will describe the sea ice model used, with section 2.1 describing standard model physics and section 2.2 describing the WIPoFSD model used. Section 3 describes the methodology used including the forcing data and model domain. Section 4 describes the results of the simulations in three sections: section 4.1 looks at the general impacts of the FSD on the sea ice; section 4.2 explores the model sensitivity to the different FSD parameters; and section 4.3 looks at the model response to a series of perturbations to the model including the wave-in-ice setup, floe shape parameter, lateral melt constants and a variable exponent. Sections 5 and 6 are the discussion and conclusion sections respectively.

2 Model description

For this study a CPOM (Centre for Polar Observation and Modelling) version of the Los Alamos Sea Ice model v 5.1.2, hereafter referred to as CICE, will be used (Hunke et al., 2015). This is a dynamic and thermodynamic sea ice model designed for inclusion within a climate model. CICE includes a large choice of different physical parameterisations. See Hunke et al. (2015) for details. Our local version also includes some state-of-the-art parameterisations not included within the CICE distribution, which will be described here. The WIPoFSD model with a waves-in-ice module implemented into standalone CICE is adapted from an implementation developed developed at the National Oceanography Centre of the UK (NOC) as a part of the EU FP7 project 'Ships and waves reaching Polar Regions (SWARP)' (Hosekova et al., 2015; NERSC, 2016) within a coupled CICE-NEMO setup. NEMO, or the Nucleus for European Modelling of the Ocean, is a state-of-the-art ocean model with applications in oceanographic research, operational oceanography, seasonal forecasts, and climate studies (Madec and the NEMO Team, 2016). This approach was originally developed to understand the impact of waves on the MIZ and the upper ocean via the thermodynamic and dynamic response. The model included the wave attenuation and floe breakup model based on the waves-ice model from the Nansen Environmental and Remote Sensing Center (NERSC) Norway, details are given by Williams et al. (2013a, 2013b). In addition, the NOC model included the following additional features: (i) a new more efficient upstream advection scheme for wave spectra (instead of the original Lax-Wendroff scheme); (ii) floe size changes due to lateral melting; (iii) floe size advection using a remapping advection scheme following Lipscomb and Hunke (2004); (iv) parameterisations for the sizes of the newly formed ice floes and (v) restoring a multiple-slope power law FSD from maximum floe sizes using a Runge-Kutta method. The features relevant to this study are described in more detail in Section 2.2. The above modelling approach was developed with a focus on the operational forecasting of the MIZ and large-scale coupled sea ice-ocean global modelling, where assuming a power law is particularly practical. The focus in this study will be on understanding the thermodynamic response of the sea ice to a power-law derived FSD and understand the individual impacts of wave-floe size and lateral melting-floe size interactions.

2.1 Description of Standard Model Physics

Within the CICE v 5.1.2 model we use the incremental remapping advection scheme (Lipscomb and Hunke, 2004), an ice thickness redistribution scheme (Lipscomb et al., 2007), along with 5 ice thickness categories (Hunke et al., 2015). The default elastic-viscous-plastic (EVP) rheology is used (Hunke and Dukowicz, 2002) along with an ice strength formulation (Rothrock, 1975). The frictional energy dissipation parameter is set to 12. A topological based melt pond scheme is used (Flocco et al., 2012) in conjunction with a Delta-Eddington radiation scheme (Briegleb and Light, 2007). The atmospheric and oceanic

neutral drag coefficients are assumed constant in time and space. An ocean heat flux formulation is used at the ice-ocean interface (Maykut and McPhee, 1995).

The rate of thermodynamic ice loss is calculated as follows (Maykut and Perovich, 1987; Steele, 1992),

$$\frac{d}{dt}(AH) = A\left[w_{top} + w_{bas} + \frac{\pi H}{\alpha L} w_{lat}\right], \quad (1)$$

where A refers to the ice area, H to the ice thickness, L refers to the floe diameter (300 m in the default set up) and α is a geometrical parameter to represent the deviation of floes from having a circular profile (0.66 in the default set up). The terms w_{top}, w_{bas} and w_{lat} refer to the melt rate at the floe upper surface (top melt), base (basal melt) and sides (lateral melt). The lateral melt rate is calculated as follows:

$$w_{lat} = m_1 \Delta T^{m_2}. \quad (2)$$

Here m_1 = 1.6 x 10^{-6} $m\ s^{-1}\ K^{-m_2}$ and m_2 = 1.36 (Perovich, 1983). The basal and top melt rates are not explicitly calculated, but instead expressed as changes in height derived from a consideration of fluxes over the top and bottom floe surfaces (Hunke et al., 2015). If the sum of the basal and lateral melts exceed the value permitted by the melt potential of the upper ocean layer within a time step, then both values will be reduced proportionally. Note that H stays constant with respect to lateral melt, so considered in isolation we have an expression for the rate of fractional ice area loss via lateral melt,

$$\frac{1}{A}\frac{dA}{dt} = \frac{\pi}{\alpha L} w_{lat.} \quad (3)$$

In these simulations, the default fixed slab ocean mixed layer (ML) is not used, and instead a prognostic mixed layer model is used wherein the temperature, salinity and depth of the layer are all able to evolve with time (Petty et al., 2014). These variables evolve based on surface fluxes and entrainment/detrainment at the base of the ML. The ML entrainment rate is calculated based on the mechanical energy input by wind forcing and surface buoyancy fluxes and profiles of water properties beneath the mixed layer (Kraus and Turner, 1967). This implementation also includes a minimum ML depth, set to 10 m.

A number of amendments are made to CICE version 5.1.2 based on recent work by Schröder et al. (2019). The maximum melt water added to melt ponds is reduced from 100 % to 50 %. This produces a more realistic distribution of melt ponds (Rösel et al., 2012). Snow erosion, to account for a redistribution of snow based on wind fields, snow density and surface topography, is parameterised based on Lecomte et al. (2015) with the additional assumptions described by Schröder et al. (2019). The 'bubbly' conductivity formulation of Pringle et al. (2007) is also included, which results in larger thermal conductivities for cooler ice.

2.2 Waves-in-ice module

The full details of this module are described in Williams et al. (2013a, 2013b), to which the reader is referred for details; here we provide an overview of the elements pertinent to our study.

The ocean surface wave spectra is taken to be given by the 2-parameter Bretschneider formula,

$$S(\omega_m, H_s) = \frac{5}{6}\frac{\omega_m^4}{\omega^5} H_s^2 e^{-\frac{5\omega_m^4}{4\omega^4}}. \quad (4)$$

Here ω is the frequency, ω_m refers to the modal frequency of the wave (both in radians per second), and H_s refers to the significant wave height (in metres). The spectra is broken down into 25 individual frequencies from a minimum wave period of 2.5 s and a maximum of 23 s.

The module operates using its own internal time-step defined by

$$t_{wav} = \frac{c\Delta x_{min}}{c_{g,max}}, \quad (5)$$

where c is the Courant-Friedrichs-Lewy (CFL) condition, here set to 0.7, Δx_{min} is the size of the smallest grid cell, and $c_{g,max}$ is the highest available group velocity. This is necessary due to the high wave-speeds observed in the Arctic. The original paper by (Williams et al., 2013b) provides further discussion of values of the CFL criterion. Over each module time step, the

wave field is advected, attenuation of waves is calculated and any ice breaking events are identified. Note also the forcing fields within each module time-step are interpolated between the prior reading and the subsequent reading to ensure smooth variations in the field (note this only applies if the grid cell remain ice-free over this period).

Once the wave field S is defined, it needs to be advected into the ice-covered regions. In the first instance this involves defining the directional space of advection. A principal direction is defined as that of the atmospheric wind direction, which should generally be a realistic (potentially less so during storm events, however). The waves are advected in 5 directions spaced equally around the principal direction, with a total spread of ± 45º. The wave field is then advected using an upwind advection scheme with each individual spectrum advected separately using its group velocity $c_g(\omega)$. This advection process is necessary because the wave forcing, derived from the ERA reanalysis data, does not cover areas with sea ice. Furthermore, due to discrepancies between the sea ice extent between the model and observations, there can exist ice-free regions within the model for which no wave forcing data is available either.

Next, the attenuation of the wave cover over each wave timestep is calculated. This will be calculated for each individual wave spectrum:

$$S_{at}(\omega) = S(\omega)e^{-\alpha_{dim}c_g(\omega)t_{wav}}, \quad (6)$$

where S_{at} is the wave spectrum after attenuation, α_{dim} is the dimensional attenuation coefficient, t_{wav} is the module timestep, and other variables are as previously defined. α_{dim} is a function of mean floe size, sea ice concentration, ice thickness and wave period (as described in Williams et al., 2013a, 2013b). The value of α_{dim} is obtained from interpolation coefficients which include both scattering and damping components, as described by Robinson and Palmer (1990). At the end of each time-step, the significant wave height and peak wave period are calculated for each grid cell where these values cannot be defined or interpolated from the forcing fields. This is achieved through integration of the wave spectra advected into each grid cell.

The model assumes that ice breaking events occur when the breaking strain amplitude E_s exceeds the breaking strain ε_c. More specifically breaking events happen when the following condition is fulfilled:

$$P(E_s > \varepsilon_c) = e^{\frac{-2\varepsilon_c^2}{E_s^2}} > P_{crit}. \quad (7)$$

Hence ice breaking events occur when the probability that the breaking strain amplitude, E_s, exceeds the breaking strain, ε_c, becomes larger than a critical probability, P_{crit}. Note that ε_c is a function of ice properties including floe size and mean ice thickness. See Williams et al. (2013a, 2013b) for further details on these parameters and how they are calculated.

2.3 Floe size distribution model

We employ a truncated power law FSD, as shown in fig. 1, described by the following equation:

$$N(x\,|d_{min} \le x \le l_{max}) = Cx^{-\alpha}. \quad (8)$$

The parameters can be defined independently for each grid cell, however in this study d_{min} and α will be fixed across the ice cover within an individual simulation, such that only l_{max} will vary in response to processes which would be expected to change the floe size. The maximum value of l_{max} is an additional constant labelled d_{max}. The constant C is defined based on the constraint imposed by total sea ice area:

$$\frac{\pi}{A}\int_{d_{min}}^{l_{max}} Nx^2\,dx = 1 \quad (9)$$

In our model there are four ways in which this distribution can be perturbed: lateral melt; break-up of floes by ocean waves; advection of floes; and restoring due to freezing. As lateral melt involves the loss of ice volume from the sides of floes, it can be expected to reduce floe size. This can be represented in the model as follows:

$$l_{max} = l_{max}\sqrt{1 - \frac{1}{A}\frac{dA}{dt}}. \quad (10)$$

The expression for fractional melt rate is now amended to

$$\frac{1}{A}\frac{dA}{dt} = \frac{\pi}{\alpha l_{eff}} w_{lat,} \quad (11)$$

where L, representing a constant floe size, has been replaced by l_{eff}, the effective floe size of the distribution. This parameter is defined in section 2.4. A floe breaking event is initiated when the conditions described in section 2.2 are fulfilled. The following amendment is applied to l_{max}:

$$l_{max} \rightarrow \max\left(d_{frag}, \frac{\lambda}{2}\right), \quad (12)$$

Where λ is the wavelength corresponding to the wave spectrum which caused the breakup.

The maximum floe size is transported using the horizontal remapping scheme with a conservative transport equation, the standard within CICE for ice area tracers (Hunke et al., 2015). An amendment to the usual scheme involves calculating a weighted average of the l_{max} over ice thickness categories post advection and subsequent mechanical redistribution. This is necessary as the parameter is not defined independently for each thickness category unlike other tracer fields.

During conditions when the model identifies frazil ice growth, it is assumed floes begin to grow. This is represented in the FSD model by the following amendment to l_{max}:

$$l_{max} \rightarrow \min\left(d_{max}, l_{max} + \frac{d_{max}\Delta t}{T_{rel}}\right), \quad (13)$$

where T_{rel} is a relaxation time which relates to how quickly the ice floes would be expected to grow to cover the entire grid cell area. It is set to 10 days as standard. Note this is a restoring approach as opposed to a physically derived parameterisation. Since the power law is the cumulative outcome of all the mechanical and thermodynamic processes that influence the FSD, some of the impact of an individual process will be tied up within the imposed power law itself.

2.4 Effective floe size

The updated lateral melt parameterisation introduced l_{eff}, the effective floe size. The effective floe size is defined as the floe size of a distribution of identical floes that would produce the same lateral melt rate in a given instant to a distribution of non-uniform floes, when under the same conditions with the same total ice cover. The lateral melt rate of a given area of sea ice is proportional to the total perimeter of that sea ice. It is hence useful to introduce a second parameter called perimeter density, ρ_P, which is the length of the ice edge per unit area of sea ice cover. The effective floe size is hence the constant floe size which produces the same ρ_P as an FSD.

First consider a probability distribution of form $Cx^{-\alpha}$. The total area of the FSD must equal to the total sea ice area i.e.

$$\varphi l^2 = \int_{d_{min}}^{l_{max}} \frac{1}{4}\pi x^2 * Cx^{-\alpha} dx, \quad (14)$$

where φl^2 refers to the total sea ice area within a grid cell (φ is the fractional ice coverage and l^2 is the total grid cell size), and the right-hand side expresses the integral of each individual floe size category in the FSD multiplied by the total ice area. We can then produce a similar expression to the integral above, but this time to find the total ice edge length, P, within a grid cell:

$$P_{fsd} = \int_{d_{min}}^{l_{max}} \pi x * Cx^{-\alpha} dx. \quad (15)$$

We can then divide the second expression by the first to get ρ_P^{fsd}, which is P divided by the total ice area in the grid cell, φl^2:

$$\rho_P^{fsd} = \frac{P_{fsd}}{\varphi l^2} = \frac{4\,(3-\alpha)[l_{max}^{2-\alpha} - d_{min}^{2-\alpha}]}{(2-\alpha)\,[l_{max}^{3-\alpha} - d_{min}^{3-\alpha}]}. \quad (16)$$

The floe shape parameter to account for deviations of floes from circular behaviour has been omitted from these expressions for clarity. This term appears as a factor in both the perimeter and area expressions and will therefore cancel out. Whilst perimeter density has not been a standard parameter to report from observations, it can be easily calculated from available FSD

data. A similar value has been reported by Perovich (2002), though this was reported per unit area of domain size (i.e. ocean plus sea ice area). We can then also define ρ_P^{con}, the perimeter density for a distribution of floes of constant size, using an analogous approach:

$$\rho_P^{con} = \frac{P_{con}}{\varphi l^2} = \frac{4}{d_{con}}. \quad (17)$$

d_{con} corresponds to the constant floe size, hence for the 300 m case we would get a perimeter density of 0.013 m^{-1}. Hence, setting the perimeter density expressions for both a constant floe size and power law FSD to be equal, and noting that this defines $d_{con} = l_{eff}$, we obtain:

$$l_{eff} = \frac{(2-\alpha)[l_{max}^{3-\alpha} - d_{min}^{3-\alpha}]}{(3-\alpha)\,[l_{max}^{2-\alpha} - d_{min}^{2-\alpha}]}. \quad (18)$$

3 Methodology

Our modified version of CICE is run over a pan-Arctic domain with a 1° tripolar (129 x 104) grid. The surface forcing is derived from the 6 hourly NCEP-2 reanalysis fields (Kanamitsu et al., 2002). The parameters that define the ocean spectra, i.e. H_s and T_p (the peak wave period used to calculate ω_m), are obtained from the ERA-interim reanalysis dataset (Dee et al., 2011). The forcings are updated at 6 hour intervals, but only for locations where the sea ice is at less than 1 % coverage i.e. grid cells where there will be negligible wave-ice interactions.

The mixed layer properties are restored over a timescale of 5 days to a monthly climatology reanalysis at 10 m depth taken from MYO-WP4-PUMGLOBAL-REANALYSIS-PHYS-001-004 (Ferry et al., 2011). This restoring is needed to effectively represent advection within the mixed layer. The deep ocean post detrainment retains the mixed layer properties, however it is restored over a timescale of 90 days to the winter climatology (herein meaning the mean of January 1st conditions from 1993-2010) from the MYO reanalysis.

All simulations are spun-up between 1st January 1990 and 31st December 2006 using the standard setup described in section 2.1 with a constant floe size of 300 m. Simulations are initiated for the 1st January 2005 using the output of the spin-up and evaluated for 12 years until 31st December 2016. A reference run is evaluated using the standard setup described in section 2.1 with a 300 m constant floe size. Figure 2 shows this model simulates the climatological monthly sea ice extent realistically for this period. All further simulations are evaluated over the same time period using the same initial model state, however with the WIPoFSD model imposed. Some simulations have additional modifications made to the model as described.

4. Results

Results are presented for the pan-Arctic domain with a focus on the melting season. All plots compare the mean behaviour over 10 years from 2007 to 2016 against the reference simulation, referred to as *ref*, which uses a constant floe size of 300 m. The results for 2005 and 2006 are discarded to allow two years for the model to adjust to the imposed FSD.

4.1 General impact of an imposed distribution

The WIPoFSD model requires the introduction of new parameters: the minimum and maximum floe size allowed and the exponent of the power law distribution. Stern et al. (2018b) were recently able to show a region of floe sizes adopting a power law with a singular exponent from 10 to 30,000 m. This is the largest range of floe sizes that a truncated power law has produced a good fit to, hence these are set as the standard values for the floe size limits in this study. For the exponent a collated analysis of observations (Stern et al., 2018a) shows a range of power laws adopted between -3.5 to -1.6 for the probability distribution (as opposed to a cumulative distribution). A standard exponent value of $\alpha = -2.5$ is adopted as an intermediate value over this range, noting in addition that this value is consistent with the ranges reported by Stern et al.

(2018b). The simulation using these standard FSD parameters, $\alpha = -2.5$, $d_{min} = 10\ m$, $d_{max} = 30{,}000\ m$, will be referred *stan-fsd* (see table 2).

Figure 3 displays the percentage difference in sea ice extent and volume for *stan-fsd* compared to *ref*. In addition, it shows the spread of twice the standard deviation of these simulations as a measure of the interannual variability. The impact on the pan-Arctic scale is small with sea ice extent and volume reductions of up to 1.2 %. The difference in sea ice area is more sensitive to melting in the early season, however the difference in sea ice volume shows a much stronger response in the peak melting season. The differences in both extent and volume evolve over an annual cycle, with minimum differences of -0.1 % and -0.2 % observed respectively between December to January for ice area and April to May for volume. The annual cycles correspond with periods of melting and freeze-up and is a product of the nature of the imposed FSD. The interannual variability shows that the impact of the WIPoFSD model with standard parameters varies significantly depending on the year. In some years the difference between the *stan-fsd* and *ref* set-ups can be negligible, in other years it can be up to 2 %. Lateral melt rates are a function of floe size but freeze-up rates are not and hence model differences only increase during periods of melting and not during periods of freeze-up. The difference in sea ice extent reduces rapidly during the freeze-up conditions; this is a consequence of the fact this lateral freeze-up behaviour is predominantly driven by ocean surface properties, which are strongly coupled to atmospheric conditions in areas of low sea ice extent. In comparison, whilst atmospheric conditions initiate the vertical sea ice growth, this atmosphere-ocean coupling is rapidly lost due to insulation of the warmer ocean from the cooler atmosphere once sea ice extends across the horizontal plane. Hence a residual difference in sea ice thickness and therefore volume propagates throughout the winter season. The difference in sea ice extent shows an additional trough in June. This feature is something also seen consistently within the data for individual years and can most likely be attributed to particular weather patterns that occur during the spring season.

Figure 4 shows the absolute difference in the mean cumulative annual melt components between the two simulations. The plot shows lateral, basal, top and total melt. A large increase can be seen in the lateral melt, however the change in total melt is negligible. This is because the lateral melt increase is largely compensated by a reduction in basal melt. The top melt also shows a negligible change. The plot also shows the change in basal melt in *stan-fsd* only accounting for the loss of basal surface area available for melting. This was calculated by multiplying the reduction in ice area in *stand-fsd* from *ref* by the basal melt rate in *ref*. The agreement (to within one standard deviation) between this synthetic reduction in basal melt and the actual reduction in basal melt suggests that the loss of ice area by lateral melt is sufficient to explain most of the basal melt compensation effect.

Figure 5 explores the spatial distribution in the changes in ice extent and volume for three months over the melting season, March, June and September. Data is shown only for regions where the sea ice cover exceeds 5 % of the total grid cell. These results show the differences increase in magnitude through the melting season. Although the pan-Arctic differences in extent and volume are marginal, Fig. 5 shows distinct regional variations in sea ice area and thickness metrics. Reductions in the fractional ice area and thickness are seen both within and beyond the MIZ with reductions of up to 0.1 and 50 cm observed respectively in September. Within the pack ice, increases in the fractional ice area of up to 0.05 and ice thickness of up to 10 cm can be seen. In September the biggest increases in thickness are directed along the North American coast, particularly within the Beaufort Sea. The distribution observed suggests the Beaufort Gyre is redistributing pack ice of higher concentration and volume to more marginal locations. In particular this appears to reverse the reduction in sea ice thickness at the outer edge of the MIZ off the Alaskan coast that is otherwise observed along the rest of the outer MIZ region. To understand the non-uniform spatial impacts of the FSD, it is useful to look at the behaviour of the effective floe size. Regions with an effective floe size greater than 300 m will experience less lateral melt than the equivalent location in *ref* (all other things being equal) whereas locations with an effective floe size below 300 m will experience more lateral melt. The distribution of this parameter is shown in Fig. 5 where in general it transitions from larger floes to smaller floes moving from the pack ice into the MIZ, with the transition to floes of a size less than 300 m observed within the MIZ. Most of the sea ice area must therefore experience

less lateral melting compared to *ref*. This result shows that the increase in lateral melt observed in Fig. 4 is very localised to regions where the ice area fraction is around 50% or below.

4.2 Exploration of the parameter space

It has been previously discussed that the floe size parameters used within the WIPoFSD model are poorly constrained by observations. In this section experiments are performed using different permutations of these parameters to assess model sensitivity to the form of the FSD.

For the first study the exponent is reduced from -2.5 to -3.5, previously identified as the most negative value within a reasonable observed range for the power law exponent. This simulation will be referred to as (A). Figure 6 is analogous to Fig. 4, comparing the component and total melt evolution for an FSD with an exponent of -3.5 compared to one with an exponent of -2.5 (with a range of 10 to 30,000 m for both). The plot shows an increase in the cumulative lateral melt, as seen before for *stan-fsd* compared to *ref*. Now, however, the basal melt is less effective at compensating this resulting in a significant increase in the total melt. There is also now a non-negligible reduction in the top melt, with the interannual variability showing the increase in total melt and reduction in top melt is consistently produced for each year of the simulations. There is a small reduction mid-annual cycle in the difference in cumulative total melt, however, implying the model with a higher exponent has an earlier melting season and a correspondingly reduced melt in the late season. The predicted change in basal melt based on the reduced sea ice area is once again plotted and it is able to account for 90% of the actual reduction in basal melt. This is in contrast to Fig. 4, where the predicted reduction in basal melt was slightly too high compared to the simulated reduction. The interannual variability shows that this underprediction of the reduction in basal melt is consistent throughout individual years. This implies the presence of additional mechanisms such as albedo and other mixed layer feedbacks causing non-negligible changes in the basal melt rate, however reduction in the ice area fraction is the leading order impact. Figure 7 shows difference map plots between the two simulations. The ice area and thickness are reduced across the sea ice cover with reductions of over 5 % and 0.5 m respectively, seen in particular locations during September. However, even in March, after the freeze-up period, reductions of 0.1 m or more in sea ice thickness can be seen within the ice pack. The response of sea ice can once again be understood through the behaviour of the effective floe size. Now this value is below 30 m across the entire ice cover throughout all three months studied, leading to increased lateral melt rates across the sea ice.

A further 17 sensitivity studies using different permutations of the parameters have been completed. These are formed by varying the three key defining parameters of the FSD shown in Fig. 1. We selected values of -2, -2.5, -3 and -3.5 for the exponent, 1 m, 20 m and 50 m for the minimum floe size and 1000 m, 10,000 m, 30,000 m and 50,000 m for the maximum floe size. These values were chosen to span the general range of values reported in studies. 14 of the 17 additional permutations are generated by selecting all the different exponent-minimum permutations (except the two already investigated). Each of these simulations has a maximum floe size of 30000 m. The further three simulations vary the maximum floe size with the exponent and minimum fixed to -2.5 and 10 m respectively. Figure 8 shows the change in mean September sea ice extent and volume relative to *ref* plotted against mean annual effective floe size. The impacts range from a small increase in extent and volume to large reductions of -22 % and -55 % respectively, even within the parameter space defined by observations. Furthermore, there is almost a one-to-one mapping between mean effective floe size and extent and volume reduction. This suggests effective floe size is a useful diagnostic tool to predict the impact of a given set of floe size parameters. The system varies most in response to the changes in the exponent, but it is also particularly sensitive to the minimum floe size.

4.3 Sensitivity runs to explore specific model components and additional relevant parameters

A series of sensitivity studies have been performed to explore the behaviour of the PL-FSD model and understand how it interacts with other model components. Table 1 defines the important parameters considered in this section and Table 2 provides a summary of the sensitivity experiments performed. The first two entries in table 2 (stan-fsd) and (ref) refer to a

standard setup using the standard FSD parameters described above and a constant floe size of 300 m respectively. Studies (A) – (C) are a selection of the simulations described in section 3.2 to allow a comparison between model sensitivity to the parameters that define the FSD and model sensitivity to other relevant parameters and components within the WIPoFSD model. In the following section a bracketed letter will follow descriptions of sensitivity studies, which corresponds to the letter assigned in table 2.

Table 3 reports key metrics for the sensitivity studies described in table 2, plus a selection of the different sensitivity studies described in section 4.2. For each experiment the September sea ice extent and volume size are reported for both the full sea ice extent and MIZ only (taken as a mean between 2007 – 2016), with the MIZ defined here as regions with between 15 and 80% sea ice cover. In addition, the mean cumulative component and total melt up until September is reported in each case, and the September mean effective floe size and mean sea ice perimeter per m^2 of ocean area are both reported for the MIZ. For each value reported (except for the effective floe size) the difference from *stan-fsd* is also stated. Cells highlighted in yellow and orange deviate by one and two standard deviation(s) respectively from the *stan-fsd* mean value (the standard deviation is calculated from the set of 10 annual values for each metric).

4.3.1 Imposing a variable exponent on the floe size distribution

The form of the FSD is defined by the exponent, α. Recent evidence suggests this may not be constant in time or space (Stern et al., 2018b). We have investigated the impact of this behaviour through the use of two alternative modelling approaches. The first approach imposes a sinusoidal annual cycle on the exponent (D):

$$\alpha = -2.35 + 0.45\cos\frac{2\pi(d-100)}{d_{ann}}. \quad (19)$$

Here d refers to the current day of the year (for example 45 would refer to 14th February) and d_{ann} is the total number of days in the year (here taken to be 365). This curve was selected as a reasonable fit to the observations of Stern et al. (2018b), though it should be noted that these observations were taken from the Beaufort and Chukchi seas so should not be assumed to be representative of the entire Arctic Ocean.

The second sensitivity experiment assumes that the exponent is a function of fractional ice area, A (E). This is derived from the observation that the exponent becomes more negative as the melting season advances and moving towards locations of lower ice cover:

$$\alpha = -4 + 2.1A. \quad (20)$$

The limits were selected to try and capture the variability of the exponent seen within observations.

The results in table 3 shows imposing the time-varying exponent (D) has a very small impact on the sea ice cover, whereas the spatial-varying exponent (E) causes a moderate reduction in September ice extent and volume of about 3 % and 5 % respectively. It is worth noting that the effective floe size is a very poor predictor in these cases of the size of the response of the system compared to cases with a fixed exponent, with the effective floe size within the MIZ much higher than expected given the size of the sea ice extent and volume reduction. The value of the mean MIZ ice perimeter is more consistent with the observed changes in sea ice extent and volume, particularly for experiment (E). This shows that it is useful to have multiple approaches to collapsing the FSD into a representative value. Whilst map plots of effective floe size can be very useful for understanding the regional impacts of an FSD, as in Fig. 5, the mean value can be misleading. Figures 9 and 10 shows how the exponent and resultant effective floe size respectively evolve in these two simulations for both the overall ice cover and the MIZ. The region spanned by twice the standard deviation of individual years within the simulation is also shown. Whilst the effective floe size in both regions behaves in corresponding ways for the simulation with a time-varying exponent (D), experiment (E) shows the mean exponent and hence effective floe size is small and approximately constant throughout the year within the MIZ, despite the overall ice pack showing strong seasonal variability for these quantities. This corresponds with earlier observations that the response of the model is particularly dependent on the behaviour of the FSD model within the MIZ. (D) shows the strongest interannual variation in effective floe size between March and May, whereas for (E) it is

strongest in the peak melting season between July and August. Figure 10 also includes the annual evolution of effective floe size for the *fsd-stan* simulation. Unlike (D) and (E), *fsd-stan* shows no strong annual oscillation in the effective floe size across the overall pack ice.

4.3.2 Other parameters affecting the floe size distribution

The two processes currently represented in the model which actively reduce floe size are lateral melting and wave induced fragmentation of floes. Two simulations are undertaken where either waves are no longer able to influence floe size (F) or lateral melting is no longer allowed to influence floe size (G). An additional three simulations are performed to focus on how waves may be influencing sea ice via reductions in floe size: the incident significant wave height at the point of entering the sea ice cover is increased by a factor of 10 (H); the floe breaking strain is reduced by a factor of 10 (I); and the wave attenuation coefficients under the sea ice are reduced by a factor of 10 (J).

The results in table 3 show that the wave-l_{max} interaction is more important than the lateral melt-l_{max} interaction in driving the increase in lateral melt observed by imposing the standard FSD. Study (F), where waves no longer break-up floes, shows a 3 % increase in MIZ volume compared to *stan-fsd*, whereas study (G), where floes do not change size as a result of lateral melt, shows an increase in MIZ volume of less than 1 %. For the three simulations performed to explore the behaviour of the wave advection model, i.e. (H), (I) and (J), the strongest response is produced by reducing the wave attenuation rate of the model (J). The weakest response is produced by increasing the ice vulnerability to wave fracture (I). Figure 11 shows difference plots of fractional ice area and effective floe size between *stan-fsd* and (J), where the attenuation rate of waves under sea ice is reduced. The plots show a reduction in the fractional ice area of around 1 % across the MIZ throughout the year for (J). This can be attributed to the reduction of the effective floe size in the same region by magnitudes of greater than 100 m. The impact can be seen within the MIZ throughout the year, even prior to the melting season in March.

The floe restoring rate is the parameter, T_{rel}, used in Eq. (12). As a standard it is set to 10 days, however this value is not well constrained. This effectively means the maximum floe size restores rapidly during freezing conditions, and hence the FSD is effectively initiated in each melting season with no memory of the previous year. There is not enough evidence available to either validate or invalidate the assumption that the FSD retains no memory of the previous melting or freeze-up season. An experiment (K) has been performed where T_{rel} is increased from 10 days to 365 days to explore the impact of inter-seasonal memory retention within the FSD model. The results in table 3 show that, whilst this change to the model did reduce the effective floe size and increase the mean MIZ perimeter density metrics by significant amounts, it did not produce a significant change in either the melt components or sea ice extent and volume.

4.3.3 Lateral melt parameters

The first order impact of introducing a variable floe size is on the lateral melt volume. Equation 1 shows the lateral melt volume is calculated from several parameters beyond just floe diameter, L, including lateral melt rate, w_{lat}, and floe shape, α. α is currently fixed to a constant value, 0.66. There has been significantly less interest in characterising how the shape of floes might vary and to characterise a floe shape distribution, particularly given available evidence suggesting floe size and shape are uncorrelated parameters (Gherardi and Lagomarsino, 2015). Two sensitivity studies are performed: one with α reduced to 0.44 (L), corresponding to 3:1 rectangular floes or similar distortions from a perfect circle; one with α increased to 0.79, corresponding to approximately circular floes (M). w_{lat} is a function of two parameters, m_1 and m_2 (see Eq. 2). These parameters have been estimated from observations and hence are subject to uncertainty. Experiments are undertaken with either both m_1 and m_2 reduced by 10% (N) or both increased by 10% (O). A reduction in these parameters reduces the lateral melt rate and an increase, the converse.

Table 3 shows that all four of these sensitivity studies did not produce a large model response in terms of the overall sea ice extent and volume. Reducing the floe shape parameter (L) produced the strongest response in the lateral melt volume, and

more generally the model metrics were more sensitive to the shape factor, α, than the melt coefficients, m_1 and m_2. The much stronger model sensitivity to the floe size parameters justifies the focus on floe size as the main uncertainty in lateral melt volume calculation.

4.3.4 Minimum mixed layer depth

The minimum ocean mixed layer depth is a constant within the prognostic mixed layer model required to prevent the mixed layer depths reaching unrealistically small values. As a standard it is set to 10 m. The depth of the mixed layer is important for the strength of mixed layer feedbacks, with a deeper mixed layer acting to damp any feedbacks via mixed layer properties. These feedbacks include the albedo feedback mechanism and the negative feedback of increased lateral and basal melts (meltwater perturbs the mixed layer properties towards less favourable melting conditions). Sensitivity studies are performed with both the minimum mixed layer depth reduced to 7 m (P) and increased to 20 m (Q).

The challenge with this particular set of experiments is that, unlike the other sensitivity studies presented here, it doesn't only act via changes in the lateral melt but will also impact the basal melt rate and sea ice freeze-up rates. Experiment (P) shows a small increase in the total sea ice extent and volume, and (Q) a small decrease, however both result in larger increases in the MIZ extent and volume. In comparison to other sensitivity studies, the changes in the lateral and basal melt are small, suggesting that mixed layer feedbacks do not have a significant role in the impacts of the FSD found in *stan-fsd* compared to *ref*. It should be noted, however, that the evidence presented here is not enough to rule out the existence of multiple compensating feedback processes.

5. Discussion

The WIPoFSD model, based on a truncated power law, has been implemented into the CPOM version of CICE 5.1.2 coupled to a prognostic mixed layer (CICE-ML model). This model assumes a fixed minimum floe size and power law exponent, but the maximum floe size evolves with respect to wave breakup (using a waves-in-ice module derived from Williams et al., 2013a, 2013b) and lateral melting. During freezing periods, the floe size is restored to its maximum value. All simulations in this study use a 15 year spin-up from 1990 to 2004 using the CICE-ML model with a constant floe size of 300 m. All experiments with the imposed WIPoFSD model are then performed from 2005 to 2016 using the output of the spin-up (*stan-fsd*), with the results from 2005 and 2006 discarded to allow the model to adjust to the new components. A reference case is also evaluated over the same time period using a constant floe size of 300 m *(ref*). A series of studies have been performed; one set exploring the parameter space constrained by observations, and one set consisting of a series of sensitivity studies to different model components and parameterisations related to the WIPoFSD model. Results showed that the imposition of the WIPoFSD with standard parameters, selected using the observations from Stern et al. (2018a, 2018b), leads to a large increase in lateral melt, however this is compensated by a reduction in the basal melt, resulting in a negligible change in the total melt. Much stronger model response was found by varying the WIPoFSD parameters to the extremes of observed ranges, in particular the minimum floe size and exponent, with extent reductions over 20 % and volume reductions of over 50 % in September compared to *ref* for the most extreme case.

It is useful to consider the physical mechanisms that drive the simulation results. It was previously noted that the increase in lateral melt observed when imposing the WIPoFSD model was compensated by a loss in basal melt, resulting in a more moderate increase in the total melt. Within the model there are three possible mechanisms causing the limited basal melt. Firstly, the increase in lateral melt will correspond to a reduction in available ice area for basal melting. It is shown in Fig. 4 and Fig. 6 that this mechanism is able to explain most of the reduction in basal melt, but the difference remains large enough that further mechanisms need to be considered. The second mechanism concerns available ocean heat. Within each timestep, the total basal melt and lateral melt is compared to the potential heat content within the upper ocean layer to see if there is sufficient heat energy available to produce the required amount of melt. If this test is failed, the basal and lateral melt are

reduced by a factor according to the available melt potential. A simulation to explore this impact shows it has only a limited impact on the basal melt, and not enough to explain the observed compensation effect. The third mechanism concerns lateral melt feedback on the basal melt rate via the perturbation of mixed layer properties. Higher freshwater release from the increase in lateral melt will lower the temperature and salinity of the ocean mixed layer, which will reduce the basal melt rate. However, the lateral melt increase also reduces the fractional ice area, lowering the albedo of the ice-ocean system. This increases the absorption of shortwave solar radiation into the mixed layer, raising the temperature of the mixed layer i.e. it has the opposite effect of the increased freshwater input. These two competing feedbacks explain the overprediction of basal melt in Fig. 4 but underprediction of basal melt in Fig. 6. The increase in total melt observed in Fig. 6 will likely correspond to a more efficient use of the available melt potential and the aforementioned albedo-feedback mechanism. The interaction between the mixed layer and FSD is further explored through the (P) and (Q) sensitivity studies where the minimum mixed layer depth was reduced and increased respectively. These studies provide further evidence that mixed layer feedbacks are not a leading order effect on the impacts of the FSD, given the very small perturbations of the melt component from the *stan-fsd* simulation. Larger changes are seen for the sea ice extent and volume metrics. However, the same mixed layer feedbacks that influence melt rates can also influence the freeze-up rate of sea ice, hence it is not possible to directly attribute these changes to WIPoFSD impacts. It should also be noted that the prognostic mixed layer model used here provides a limited representation of sea ice-ocean interactions and feedbacks. The strength of these interactions may increase within a fully coupled sea ice-ocean model (Rynders, 2017).

The series of sensitivity studies to both the floe size parameters and other aspects of the WIPoFSD model are useful to understand the limitations of the model. An important result is the limited sensitivity of the model to the m_1, m_2, and α_{shape} parameters, i.e. experiments (L) – (O), with significant perturbations of these parameters reducing the sea ice extent by around 1 % or less. Given these are additional constants needed to calculate the lateral melt rate beyond floe size, if a strong sensitivity was found to these parameters it would imply that imposing a floe size distribution was introducing unnecessary complexity into the parameterisation where some other component was dominating the uncertainty within this parameterisation. This justifies the focus on floe size as opposed to the other components of the lateral melt calculation. Experiment (K) showed very little model response to increasing the floe freeze-up timescale, T_{rel}, from 10 to 365 days. This result suggests that the use of more physically derived parameterisations of the floe growth during freezing conditions (e.g. Roach et al., 2018b) would not have a significant impact within the model framework presented here.

The sensitivity studies also give insight into the impact of waves on the sea ice cover. In particular, the two sensitivity studies that switch off the lateral melt-floe size (G) and wave-floe size feedback (F) mechanisms respectively showed that the latter was more important for the observed changes in sea ice area and extent when imposing the WIPoFSD with standard parameters. This impact was enhanced through various perturbations to the wave model. The increase in significant wave height (H) and reduction in ice strength (I) are representative of future Arctic conditions when the sea ice is expected to be thinner (Aksenov et al., 2017) with storms of increasing strength and duration (Basu et al., 2018). The results presented here suggest that these changes will have only a limited impact on sea ice extent and volume via the floe size feedback mechanism. The strongest response in sea ice extent and volume was observed with a reduction in the attenuation rate (J). Modelling the propagation and energy loss of waves as they travel under sea ice is a complex problem and an area of active research (Meylan et al., 2017), and there are recent efforts to produce coupled wave-sea ice models (Herman, 2017). However, any increase in complexity in modelling the waves will result in increased computational cost. Further observations about wave attenuation in sea ice are needed to judge the complexity of the model approach required to produce sufficient accuracy.

As stated above, the model shows a strong sensitivity to the floe size parameters with some selections of the WIPoFSD parameters showing moderate increases in the sea ice extent and volume, and other selections driving reductions of these values by over 50 % in September. The limited observational data available to constrain the selected parameters is a significant challenge of this modelling approach. Furthermore, a not insignificant model response of order 5% relative to *ref* has been

observed to sensitivity experiment (E) performed here to explore the impacts of the non-uniform exponent observed by Stern et al. (2018a). The WIPoFSD model used here assumes a truncated power law distribution with a fixed exponent, minimum floe size and global maximum floe size. Each grid cell has a locally defined grid cell which is perturbed in response to wave break-up events, lateral melt, and freezing conditions. The prognostic model approach used by Roach et al. (2018a) would avoid making such strong assumptions about the form of the FSD and provides a more flexible framework to understand the factors that determine these different parameters and why floe size tends to adopt a power law. For example, it can be used to understand what factors may drive intra-annual changes in the exponent, something not possible in the framework described here as the exponent is prescribed. However, new physical parametrisations will introduce new constants that will have to be constrained from observations. Furthermore, given the large knowledge gaps regarding processes that impact floe size, a model that can easily be constrained by observations i.e. the WIPoFSD model, may be the preferred approach for more general applications. This will be particularly true if upcoming studies, including MOSAiC, provide further observational evidence to support the use of a power law and provide data to better constrain the WIPoFSD parameters. In addition, the identification of the effective floe size as a useful floe size parameter may provide a method to report useful FSD information over a larger spatial and temporal scale, as this value can be calculated from the ice perimeter length within a unit area and avoids the need to report a full distribution. This would allow an assessment of the regional, intra-annual and inter-annual variability of the FSD and identify the FSD parameters and components that best reproduce these desired features.

One of the key impacts of the use of an WIPoFSD was the non-uniform impact on the ice cover, with an enhancement in lateral melt and reduction in ice volume within the MIZ, as shown in Fig. 5. The reference simulation used here currently underpredicts summer ice concentration in the pack ice but overpredicts the concentration at the ice edge, consistent with other studies that use the CICE sea ice model (such as Schröder et al., 2019). An analysis of the historically forced simulations used within phase 5 of the Coupled Model Intercomparison Project (CMIP5) found that coupled models consistently performed poorly in capturing the regional variation in sea ice concentration, showing this problem isn't specific to CPOM CICE simulations (Ivanova et al., 2016). This suggests that models currently underestimate the role of the MIZ in driving the seasonal sea ice loss, and one of the observed features of the imposed WIPoFSD model is the enhancement of lateral melt in this region. Whilst the changes are generally small, it shows that the use of an FSD model, either in the described form or otherwise, may be an important step towards improving the accuracy of sea ice models.

6. Conclusion

Climate model representations of sea ice currently assume that the size of floes that make up the sea ice is constant; however, observations show that floes adopt a distribution of sizes. A truncated power law generally produces a good fit to observations of the floe size distribution (FSD), though the size range and exponent reported for this distribution vary significantly between different studies. A power law derived FSD model including a waves-in-ice module (WIPoFSD) has been imposed into the Los Alamos sea ice model coupled to a prognostic mixed layer model, CICE-ML. The WIPoFSD is defined by the minimum floe size, maximum floe size and exponent. In this model the maximum floe size varies in response to lateral melting, wave breakup events and freezing conditions. The minimum floe size and exponent are fixed. A standard set of parameters for the WIPoFSD model is identified from observations and the results of a sea ice simulation using these parameters is compared to one with a constant floe size of 300 m. Inclusion of the WIPoFSD model within CICE-ML results in increased lateral melt compensated by reductions in basal melt, resulting in only moderate impacts on the total melt. The primary mechanism by which the increased lateral melt reduces the basal melt is shown to be the reduction in available ice area for basal melt. The impact is not spatially homogeneous, with losses in sea ice area and volume dominating in the marginal ice zone (MIZ). These impacts partially correct existing model biases in the standalone CICE-ML model, suggesting the inclusion of an FSD is an important step forward in ensuring that models can produce realistic simulations of the Arctic sea ice.

A series of sensitivity experiments explore the limitations of the model. The model does show a strong response to a reduction in wave attenuation rate, suggesting this is an important component in understanding wave-sea ice interactions. Different selections of parameters for the WIPoFSD show a large variability in their response, with some showing a moderate increase in mean September sea ice extent and volume, with others reducing these metrics by over 20 and 50 % respectively. A newly defined parameter, effective floe size, is found to be a good predictor of model response for simulations where the minimum floe size and power law exponent are fixed. The impact of a non-uniform exponent was also explored based on observations that these parameters evolve for a given region of ice. Results suggest that this parameter could further enhance the differential behaviour seen between pack ice and the MIZ in response to the imposition of an FSD. These sensitivity studies also showed that the choice of WIPoFSD parameters are a source of much larger uncertainty to the model than other constants used within the lateral melt parameterisation, justifying the focus on developing an FSD model as a priority for improved accuracy of sea ice modelling.

Whilst the model presented here does make a major assumption that the floe size distribution adopts a power law, this is consistent with the majority of observations. Furthermore, it has been shown that the model can be easily modified to adapt to additional findings such as the inclusion of a non-uniform exponent. This means the WIPoFSD model is a useful tool for assessing the importance of the FSD in the evolution of sea ice, particularly the seasonal retreat. Its simplicity also means it is a useful candidate as a modelling approach to represent the FSD in climate models, where there is an important balance to be maintained between physical fidelity and computational expense. Whilst the model is currently limited by too little observational data to constrain the FSD parameters, planned studies such a MOSAiC should enable much stronger constraints to be placed on these parameters.

Data Availability

TBC

Author Contributions

LH, with support from YA, developed the original version of the WIPoFSD model with a coupled CICE-NEMO framework. DS adapted the model into the CPOM CICE standalone setup. AB further developed the WIPoFSD model and completed the simulations and analysis under the supervision of DF, DS, LH, JR and YA. DS provided additional technical support. AB composed the paper with feedback and contributions from all authors.

Competing interests

The authors declare that they have no conflict of interest.

Acknowledgements

AB is funded through a NERC industrial CASE studentship with the UK Met Office, reference NE/M009637/1. The contributions of DF and DS were supported by NERC grant, number NE/R016690/. JR is supported by the Joint UK BEIS/Defra Met Office Hadley Centre Climate Programme (GA01 101). LH and YA acknowledge support from European Union Seventh Framework Programme SWARP (Grant agreement 607476). YA was also supported by “Towards a marginal Arctic sea ice cover” NE/R000654/1. LH and YA would also like to express gratitude towards Dr Timothy D. Williams (Nansen Environmental and Remote Sensing Center, NERSC, Norway), Prof. Dany Dumont (Institut des sciences de la mer de Rimouski, Québec, Canada), and Prof. Vernon A. Squire (University of Otago, New Zealand) for their kind advice on ice-waves interaction. Dr Stefanie Rynders (National Oceanography Centre, Southampton) should also receive credit for also contributing to the development of the WIPoFSD model within the coupled CICE-NEMO framework alongside LH and YA.

Coupled CICE-NEMO simulations were performed on the ARCHER UK National Supercomputing Service (http://www.archer.ac.uk).

References

Aksenov, Y., Popova, E. E., Yool, A., Nurser, A. J. G., Williams, T. D., Bertino, L. and Bergh, J.: On the future navigability of Arctic sea routes: High-resolution projections of the Arctic Ocean and sea ice, Mar. Policy, doi:10.1016/j.marpol.2015.12.027, 2017.

Basu, S., Zhang, X. and Wang, Z.: Eurasian Winter Storm Activity at the End of the Century: A CMIP5 Multi-model Ensemble Projection, Earth's Futur., 6(1), 61–70, doi:10.1002/2017EF000670, 2018.

Bennetts, L. G., O'Farrell, S. and Uotila, P.: Brief communication: Impacts of ocean-wave-induced breakup of Antarctic sea ice via thermodynamics in a stand-alone version of the CICE sea-ice model, Cryosphere, doi:10.5194/tc-11-1035-2017, 2017.

Boutin, G., Ardhuin, F., Dumont, D., Sévigny, C., Girard-Ardhuin, F. and Accensi, M.: Floe Size Effect on Wave-Ice Interactions: Possible Effects, Implementation in Wave Model, and Evaluation, J. Geophys. Res. Ocean., 123(7), 4779–4805, doi:10.1029/2017JC013622, 2018.

Briegleb, B. P. and Light, B.: A Delta-Eddington Multiple Scattering Parameterization For Solar Radiation In The Sea Ice Component Of The Community Climate System Model, NCAR Tech. Note, doi:10.5065/D6B27S71, 2007.

Curry, J. A., Schramm, J. L. and Ebert, E. E.: Sea ice-albedo climate feedback mechanism, J. Clim., doi:10.1175/1520-0442(1995)008<0240:SIACFM>2.0.CO;2, 1995.

Dee, D. P., Uppala, S. M., Simmons, A. J., Berrisford, P., Poli, P., Kobayashi, S., Andrae, U., Balmaseda, M. A., Balsamo, G., Bauer, P., Bechtold, P., Beljaars, A. C. M., van de Berg, L., Bidlot, J., Bormann, N., Delsol, C., Dragani, R., Fuentes, M., Geer, A. J., Haimberger, L., Healy, S. B., Hersbach, H., Hólm, E. V., Isaksen, L., Kållberg, P., Köhler, M., Matricardi, M., Mcnally, A. P., Monge-Sanz, B. M., Morcrette, J. J., Park, B. K., Peubey, C., de Rosnay, P., Tavolato, C., Thépaut, J. N. and Vitart, F.: The ERA-Interim reanalysis: Configuration and performance of the data assimilation system, Q. J. R. Meteorol. Soc., 137(656), 553–597, doi:10.1002/qj.828, 2011.

Dethloff, K., Rex, M. and Shupe, M.: Multidisciplinary Drifting Observatory for the Study of Arctic Climate (MOSAiC), in EGU General Assembly Conference Abstracts, vol. 18., 2016.

Dickinson, R. E., Meehl, G. A. and Washington, W. M.: Ice-albedo feedback in a CO2-doubling simulation, Clim. Change, 10(3), 241–248, doi:10.1007/BF00143904, 1987.

Ferry, N., Masina, S., Storto, A., Haines, K., Valdivieso, M., Barnier, B. and Molines, J.-M.: Product user manual global-reanalysis-phys-001-004-a and b, myocean., Tech. rep., 2011.

Flocco, D., Schroeder, D., Feltham, D. L. and Hunke, E. C.: Impact of melt ponds on Arctic sea ice simulations from 1990 to 2007, J. Geophys. Res. Ocean., doi:10.1029/2012JC008195, 2012.

Gherardi, M. and Lagomarsino, M. C.: Characterizing the size and shape of sea ice floes, Sci. Rep., 5, 1–11, doi:10.1038/srep10226, 2015.

Hauser, D. D. W., Laidre, K. L., Stafford, K. M., Stern, H. L., Suydam, R. S. and Richard, P. R.: Decadal shifts in autumn migration timing by Pacific Arctic beluga whales are related to delayed annual sea ice formation, Glob. Chang. Biol., doi:10.1111/gcb.13564, 2017.

Herman, A.: Sea-ice floe-size distribution in the context of spontaneous scaling emergence in stochastic systems, Phys. Rev. E - Stat. Nonlinear, Soft Matter Phys., 81(6), 1–5, doi:10.1103/PhysRevE.81.066123, 2010.

Herman, A.: Wave-induced stress and breaking of sea ice in a coupled hydrodynamic discrete-element wave-ice model, Cryosphere, doi:10.5194/tc-11-2711-2017, 2017.

Herman, A.: Wave-Induced Surge Motion and Collisions of Sea Ice Floes: Finite-Floe-Size Effects, J. Geophys. Res. Ocean.,

doi:10.1029/2018JC014500, 2018.

Herman, A., Evers, K. U. and Reimer, N.: Floe-size distributions in laboratory ice broken by waves, Cryosphere, doi:10.5194/tc-12-685-2018, 2018.

Ho, J.: The implications of Arctic sea ice decline on shipping, Mar. Policy, 34(3), 713–715, doi:10.1016/j.marpol.2009.10.009, 2010.

Horvat, C. and Tziperman, E.: A prognostic model of the sea-ice floe size and thickness distribution, Cryosphere, 9(6), 2119–2134, doi:10.5194/tc-9-2119-2015, 2015.

Horvat, C. and Tziperman, E.: The evolution of scaling laws in the sea ice floe size distribution, J. Geophys. Res. Ocean., doi:10.1002/2016JC012573, 2017.

Horvat, C. and Tziperman, E.: Understanding Melting due to Ocean Eddy Heat Fluxes at the Edge of Sea-Ice Floes, Geophys. Res. Lett., doi:10.1029/2018GL079363, 2018.

Hosekova, L., Aksenov, Y., Coward, A., Williams, T., Bertino, L. and Nurser, A. J. G.: Modelling Sea Ice and Surface Wave Interactions in Polar Regions, in AGU Fall Meeting Abstracts, p. GC34A–06, San Francisco., 2015.

Hunke, E. and Dukowicz, J.: The elastic-viscous-plastic sea ice dynamics model in general orthogonal curvilinear coordinates on a sphere-incorporation of metric terms, D R A F T Oct., doi:10.1175/1520-0493(2002)130<1848:TEVPSI>2.0.CO;2, 2002.

Hunke, E. C., Lipscomb, W. H., Turner, A. K., Jeffery, N. and Elliott, S.: CICE : the Los Alamos Sea Ice Model Documentation and Software User ' s Manual LA-CC-06-012, , 115, 2015.

Hwang, B., Wilkinson, J., Maksym, E., Graber, H. C., Schweiger, A., Horvat, C., Perovich, D. K., Arntsen, A. E., Stanton, T. P., Ren, J. and Wadhams, P.: Winter-to-summer transition of Arctic sea ice breakup and floe size distribution in the Beaufort Sea, Elem Sci Anth, 5(0), 40, doi:10.1525/elementa.232, 2017.

Ivanova, D. P., Gleckler, P. J., Taylor, K. E., Durack, P. J. and Marvel, K. D.: Moving beyond the total sea ice extent in gauging model biases, J. Clim., doi:10.1175/JCLI-D-16-0026.1, 2016.

Kanamitsu, M., Ebisuzaki, W., Woollen, J., Yang, S. K., Hnilo, J. J., Fiorino, M. and Potter, G. L.: NCEP-DOE AMIP-II reanalysis (R-2), Bull. Am. Meteorol. Soc., doi:10.1175/BAMS-83-11-1631(2002)083<1631:NAR>2.3.CO;2, 2002.

Kraus, E. B. and Turner, J. S.: A one-dimensional model of the seasonal thermocline II. The general theory and its consequences, Tellus, doi:10.3402/tellusa.v19i1.9753, 1967.

Kwok, R.: Arctic sea ice thickness, volume, and multiyear ice coverage: Losses and coupled variability (1958-2018), Environ. Res. Lett., doi:10.1088/1748-9326/aae3ec, 2018.

Laidler, G. J., Ford, J. D., Gough, W. A., Ikummaq, T., Gagnon, A. S., Kowal, S., Qrunnut, K. and Irngaut, C.: Travelling and hunting in a changing Arctic: Assessing Inuit vulnerability to sea ice change in Igloolik, Nunavut, Clim. Change, doi:10.1007/s10584-008-9512-z, 2009.

Lecomte, O., Fichefet, T., Flocco, D., Schroeder, D. and Vancoppenolle, M.: Interactions between wind-blown snow redistribution and melt ponds in a coupled ocean-sea ice model, Ocean Model., doi:10.1016/j.ocemod.2014.12.003, 2015.

Lee, C. M., Cole, S., Doble, M., Freitag, L., Hwang, P., Jayne, S., Jeffries, M., Krishfield, R., Maksym, T., Maslowski, W., Owens, B., Posey, P., Rainville, L., Roberts, A., Shaw, B., Stanton, T., Thomson, J., Timmermans, M., Toole, J., Wadhams, P., Wilkinson, J. and Zhang, J.: Marginal Ice Zone (MIZ) Program : Science and Experiment Plan APL-UW 1201 October 2012 Applied Physics Laboratory University of Washington, , (October 2012), 2012.

Lipscomb, W. H. and Hunke, E. C.: Modeling Sea Ice Transport Using Incremental Remapping, Mon. Weather Rev., 132(6), 1341–1354, doi:10.1175/1520-0493(2004)132<1341:MSITUI>2.0.CO;2, 2004.

Lipscomb, W. H., Hunke, E. C., Maslowski, W. and Jakacki, J.: Ridging, strength, and stability in high-resolution sea ice models, J. Geophys. Res. Ocean., doi:10.1029/2005JC003355, 2007.

Liu, A. K., Vachon, P. W., Peng, C. Y. and Bhogal, A. S.: Wave attenuation in the marginal ice zone during limex, Atmos. - Ocean, doi:10.1080/07055900.1992.9649437, 1992.

Lüpkes, C., Gryanik, V. M., Hartmann, J. and Andreas, E. L.: A parametrization, based on sea ice morphology, of the neutral atmospheric drag coefficients for weather prediction and climate models, J. Geophys. Res. Atmos., 117(13), 1–18, doi:10.1029/2012JD017630, 2012.

Madec, G. and the NEMO Team: NEMO ocean engine, in Note du Pôle de modélisation., 2016.

Maslanik, J. A., Fowler, C., Stroeve, J., Drobot, S., Zwally, J., Yi, D. and Emery, W.: A younger, thinner Arctic ice cover: Increased potential for rapid, extensive sea-ice loss, Geophys. Res. Lett., doi:10.1029/2007GL032043, 2007.

Maykut, G. A. and McPhee, M. G.: Solar heating of the Arctic mixed layer, J. Geophys. Res., doi:10.1029/95JC02554, 1995.

Maykut, G. A. and Perovich, D. K.: The role of shortwave radiation in the summer decay of a sea ice cover, J. Geophys. Res. Ocean., 92(C7), 7032–7044, doi:10.1029/JC092iC07p07032, 1987.

McPhee, M. G., Maykut, G. A. and Morison, J. H.: Dynamics and thermodynamics of the ice/upper ocean system in the marginal ice zone of the Greenland Sea, J. Geophys. Res. Ocean., doi:10.1029/JC092iC07p07017, 1987.

Meylan, M. and Squire, V. A.: The response of ice floes to ocean waves, J. Geophys. Res., doi:10.1029/93JC02695, 1994.

Meylan, M. H., Bennetts, L. G. and Peter, M. A.: Water-wave scattering and energy dissipation by a floating porous elastic plate in three dimensions, Wave Motion, doi:10.1016/j.wavemoti.2016.06.014, 2017.

NERSC: Ships and Waves Reaching Polar Regions D5 . 1 Validation Reports, Bergen. [online] Available from: Ships and Waves Reaching Polar regions, 2016.

Notz, D. and Stroeve, J.: The Trajectory Towards a Seasonally Ice-Free Arctic Ocean, Curr. Clim. Chang. Reports, doi:10.1007/s40641-018-0113-2, 2018.

Parkinson, C. L. and Cavalieri, D. J.: Antarctic sea ice variability and trends, 1979-2010, Cryosphere, doi:10.5194/tc-6-871-2012, 2012.

Perovich, D. K.: On the summer decay of a sea ice cover., 1983.

Perovich, D. K.: Aerial observations of the evolution of ice surface conditions during summer, J. Geophys. Res., doi:10.1029/2000JC000449, 2002.

Petty, A. A., Holland, P. R. and Feltham, D. L.: Sea ice and the ocean mixed layer over the Antarctic shelf seas, Cryosphere, 8(2), 761–783, doi:10.5194/tc-8-761-2014, 2014.

Post, E., Forchhammer, M. C., Bret-Harte, M. S., Callaghan, T. V., Christensen, T. R., Elberling, B., Fox, A. D., Gilg, O., Hik, D. S., Høye, T. T., Ims, R. A., Jeppesen, E., Klein, D. R., Madsen, J., McGuire, A. D., Rysgaard, S., Schindler, D. E., Stirling, I., Tamstorf, M. P., Tyler, N. J. C., Van Der Wal, R., Welker, J., Wookey, P. A., Schmidt, N. M. and Aastrup, P.: Ecological dynamics across the arctic associated with recent climate change, Science (80-.)., doi:10.1126/science.1173113, 2009.

Pringle, D. J., Eicken, H., Trodahl, H. J. and Backstrom, L. G. E.: Thermal conductivity of landfast Antarctic and Arctic sea ice, J. Geophys. Res. Ocean., doi:10.1029/2006JC003641, 2007.

Regehr, E. V., Hunter, C. M., Caswell, H., Amstrup, S. C. and Stirling, I.: Survival and breeding of polar bears in the southern Beaufort Sea in relation to sea ice, J. Anim. Ecol., doi:10.1111/j.1365-2656.2009.01603.x, 2010.

Roach, L. A., Horvat, C., Dean, S. M. and Bitz, C. M.: An Emergent Sea Ice Floe Size Distribution in a Global Coupled Ocean-Sea Ice Model, J. Geophys. Res. Ocean., doi:10.1029/2017JC013692, 2018a.

Roach, L. A., Smith, M. M. and Dean, S. M.: Quantifying Growth of Pancake Sea Ice Floes Using Images From Drifting Buoys, J. Geophys. Res. Ocean., 123(4), 2851–2866, doi:10.1002/2017JC013693, 2018b.

Robinson, N. J. and Palmer, S. C.: A modal analysis of a rectangular plate floating on an incompressible liquid, J. Sound Vib., doi:10.1016/0022-460X(90)90661-I, 1990.

Rösel, A., Kaleschke, L. and Birnbaum, G.: Melt ponds on Arctic sea ice determined from MODIS satellite data using an artificial neural network, Cryosphere, doi:10.5194/tc-6-431-2012, 2012.

Rothrock, D. A.: The energetics of the plastic deformation of pack ice by ridging, J. Geophys. Res., doi:10.1029/JC080i033p04514, 1975.

Rothrock, D. a and Thorndike, A. S.: Measuring the sea ice floe size distribution, J. Geophys. Res., 89, 6477–6486, doi:10.1029/JC089iC04p06477, 1984.

Rynders, S.: Impact of surface waves on sea ice and ocean in the polar regions, University of Southampton, United Kingdom., 2017.

Schröder, D., Feltham, D. L., Tsamados, M., Ridout, A. and Tilling, R.: New insight from CryoSat-2 sea ice thickness for sea ice modelling, Cryosph. Discuss., 1–25, doi:10.5194/tc-2018-159, 2019.

Screen, J. A., Simmonds, I., Deser, C. and Tomas, R.: The atmospheric response to three decades of observed arctic sea ice loss, J. Clim., doi:10.1175/JCLI-D-12-00063.1, 2013.

Sepp, M. and Jaagus, J.: Changes in the activity and tracks of Arctic cyclones, Clim. Change, doi:10.1007/s10584-010-9893-7, 2011.

Smith, L. C. and Stephenson, S. R.: New Trans-Arctic shipping routes navigable by midcentury, Proc. Natl. Acad. Sci., doi:10.1073/pnas.1214212110, 2013.

Squire, V. A.: Of ocean waves and sea-ice revisited, Cold Reg. Sci. Technol., doi:10.1016/j.coldregions.2007.04.007, 2007.

Steele, M.: Sea ice melting and floe geometry in a simple ice-ocean model, J. Geophys. Res. Ocean., doi:10.1029/92JC01755, 1992.

Steer, A., Worby, A. and Heil, P.: Observed changes in sea-ice floe size distribution during early summer in the western Weddell Sea, Deep. Res. Part II Top. Stud. Oceanogr., 55(8–9), 933–942, doi:10.1016/j.dsr2.2007.12.016, 2008.

Stern, H. L., Schweiger, A. J., Zhang, J. and Steele, M.: On reconciling disparate studies of the sea-ice floe size distribution, Elem Sci Anth, doi:10.1525/elementa.304, 2018a.

Stern, H. L., Schweiger, A. J., Stark, M., Zhang, J., Steele, M. and Hwang, B.: Seasonal evolution of the sea-ice floe size distribution in the Beaufort and Chukchi seas, Elem Sci Anth, 6(1), 48, doi:10.1525/elementa.305, 2018b.

Stopa, J. E., Ardhuin, F. and Girard-Ardhuin, F.: Wave climate in the Arctic 1992-2014: Seasonality and trends, Cryosphere, 10(4), 1605–1629, doi:10.5194/tc-10-1605-2016, 2016.

Stroeve, J. and Notz, D.: Changing state of Arctic sea ice across all seasons, Environ. Res. Lett., doi:10.1088/1748-9326/aade56, 2018.

Stroeve, J. C., Schroder, D., Tsamados, M. and Feltham, D.: Warm winter, thin ice?, Cryosphere, doi:10.5194/tc-12-1791-2018, 2018.

Thomson, J. and Lee, C.: An autonomous approach to observing the seasonal ice zone in the western Arctic, Oceanography, doi:10.5670/oceanog.2017.222, 2017.

Toyota, T., Kohout, A. and Fraser, A. D.: Formation processes of sea ice floe size distribution in the interior pack and its relationship to the marginal ice zone off East Antarctica, Deep. Res. Part II Top. Stud. Oceanogr., 131, 28–40, doi:10.1016/j.dsr2.2015.10.003, 2016.

Tsamados, M., Feltham, D., Petty, A., Schroder, D. and Flocco, D.: Processes controlling surface, bottom and lateral melt of Arctic sea ice in a state of the art sea ice model, , 17, 10302, doi:10.1098/rsta.2014.0167, 2015.

Vihma, T.: Effects of Arctic Sea Ice Decline on Weather and Climate: A Review., 2014.

Williams, T. D., Bennetts, L. G., Squire, V. A., Dumont, D. and Bertino, L.: Wave-ice interactions in the marginal ice zone. Part 1: Theoretical foundations, Ocean Model., 71, 81–91, doi:10.1016/j.ocemod.2013.05.010, 2013a.

Williams, T. D., Bennetts, L. G., Squire, V. A., Dumont, D. and Bertino, L.: Wave-ice interactions in the marginal ice zone. Part 2: Numerical implementation and sensitivity studies along 1D transects of the ocean surface, Ocean Model., 71, 92–101, doi:10.1016/j.ocemod.2013.05.011, 2013b.

Winton, M.: Amplified Arctic climate change: What does surface albedo feedback have to do with it?, Geophys. Res. Lett., 33(3), 1–4, doi:10.1029/2005GL025244, 2006.

Winton, M.: Sea Ice-Albedo Feedback and Nonlinear Arctic Climate Change, in Arctic Sea Ice Decline: Observations,

Projections, Mechanisms, and Implications., 2013.

Young, I. R., Zieger, S. and Babanin, A. V.: Global trends in wind speed and wave height, Science (80-.)., doi:10.1126/science.1197219, 2011.

Zhang, J., Lindsay, R., Schweiger, A. and Rigor, I.: Recent changes in the dynamic properties of declining Arctic sea ice: A model study, Geophys. Res. Lett., doi:10.1029/2012GL053545, 2012.

Zhang, J., Schwinger, A., Steele, M. and Stern, H.: Sea ice floe size distribution in the marginal ice zone: Theory and numerical experiments, J Geophys Res, 120, 3484–3498, doi:10.1002/2015JC010770.Received, 2015.

The Cryosphere Discuss., https://doi.org/10.5194/tc-2019-44
Manuscript under review for journal The Cryosphere
Discussion started: 21 March 2019

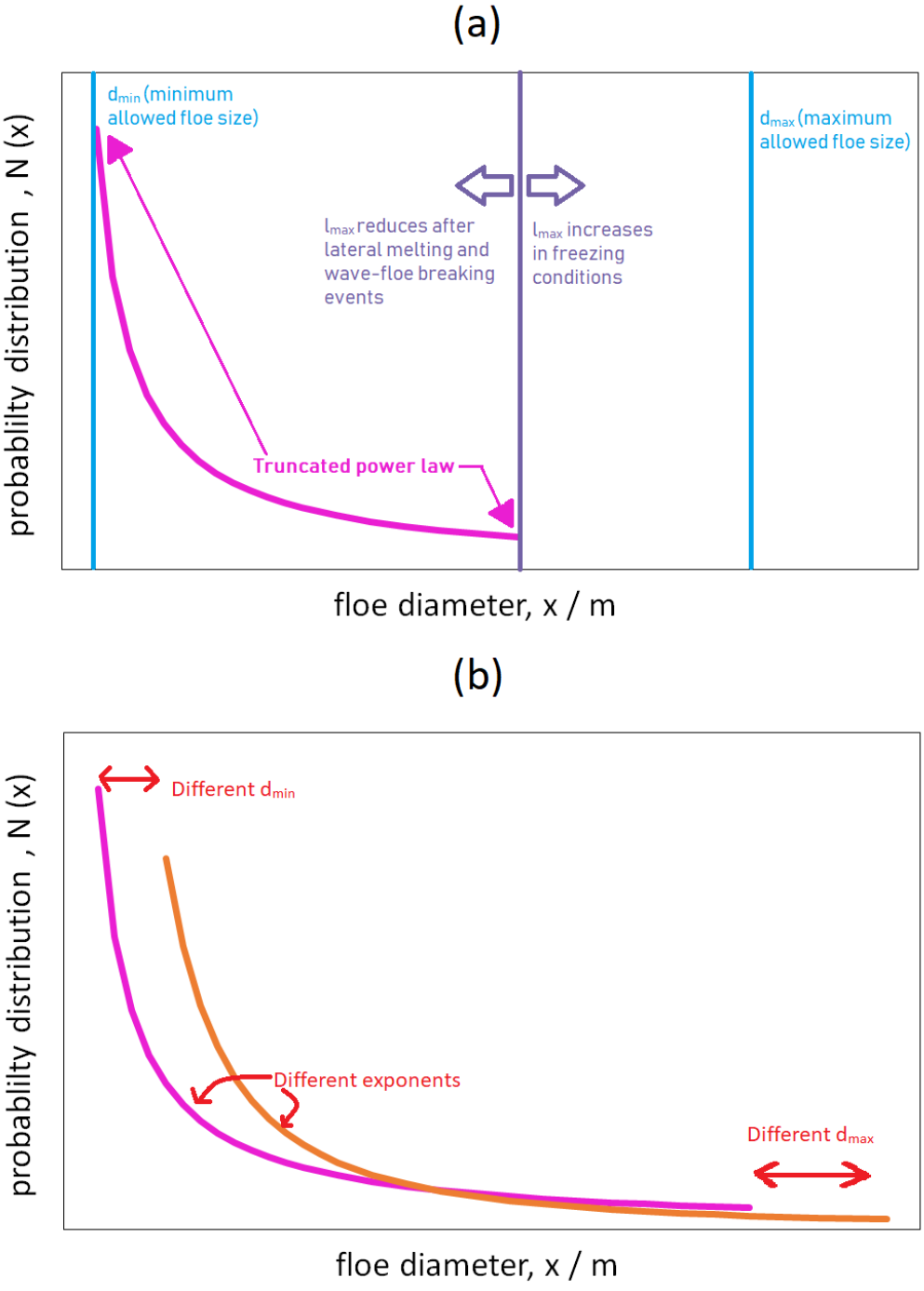

Figure 1: Panel (a) is a schematic of the imposed FSD model. This model is initiated by prescribing a truncated power law with an exponent, α, and between the limits d_{min} and $d_{max,}$ where d_{max} sets the maximum limit of the power law. Within individual grid cells the maximum floe size is not fixed and varies between these two limits. The local maximum floe size, l_{max}, evolves through lateral melting, wave breakup events and freezing. Panel (b) shows the how d_{min}, d_{max} and α can all be varied to produce different distributions.

The Cryosphere Discuss., https://doi.org/10.5194/tc-2019-44
Manuscript under review for journal The Cryosphere
Discussion started: 21 March 2019

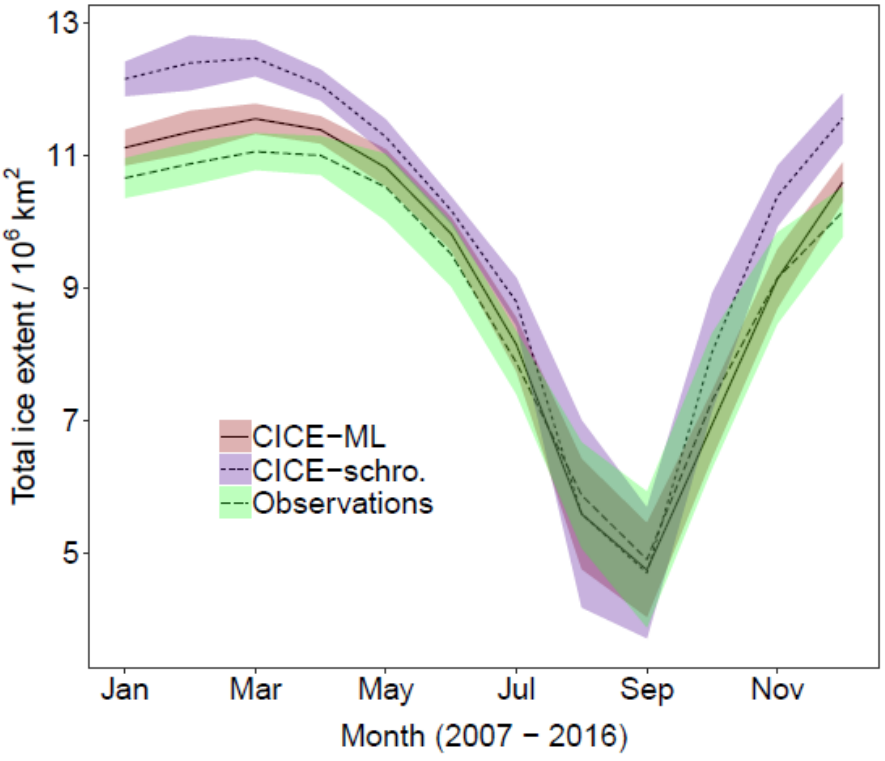

Figure 2: Comparison of the 2007 – 2016 mean cycle for the total Arctic sea ice extent simulated in the coupled CICE-prognostic mixed layer reference setup (marked CICE-ML, red ribbon, solid) with the results from the standard optimised CPOM CICE model (Schröder et al., marked CICE-schro., 2018, blue ribbon, small dashes) and observed sea ice extent derived from Nimbus-7 SMMR and DMSP SSM/I-SSMIS satellites using Bootstrap algorithm version 3 (Comiso, 2017, marked Observations, green ribbon, large dashes). The ribbon shows, in each case, the region spanned by the mean value plus or minus two times the standard deviation for each simulation. This gives a measure of the interannual variability over the 10-year period. Results show the new model performs either comparably to or better than the previous optimum setup throughout the year. In addition, the mean CICE-ML sea ice extent falls within the interannual variability of the observations between June and December i.e. most of the melting season, suggesting this reference state is suitable for studies focusing on this period.

The Cryosphere Discuss., https://doi.org/10.5194/tc-2019-44
Manuscript under review for journal The Cryosphere
Discussion started: 21 March 2019

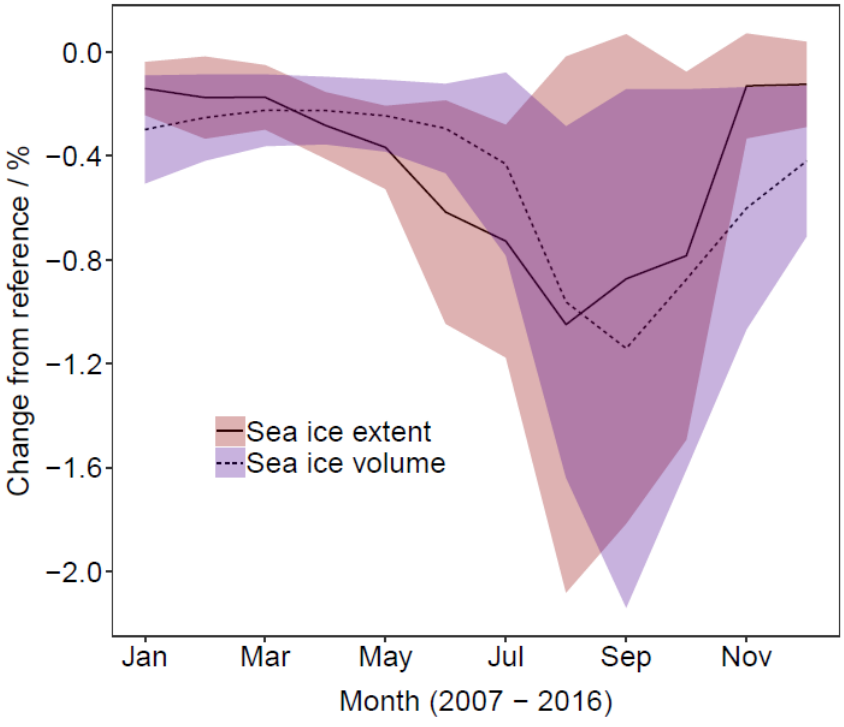

Figure 3: Difference in sea ice extent (solid, red ribbon) and volume (dashed, blue ribbon) between *stan-fsd* relative to *ref* (using a constant floe size) averaged over 2007 - 2016. The ribbon shows, in each case, the region spanned by the mean value plus or minus two times the standard deviation for each simulation. This gives a measure of the interannual variability over the 10-year period. The mean behaviour is a reduction in the sea ice extent and volume, with losses of up to 1 % and 1.2 % respectively seen in September during the period of minimum sea ice. The interannual variability shows that the impact of the WIPoFSD model with standard parameters varies significantly between years, with some years potentially showing negligible change in extent and volume and others showing a maximum reduction of over 2 %.

The Cryosphere Discuss., https://doi.org/10.5194/tc-2019-44
Manuscript under review for journal The Cryosphere
Discussion started: 21 March 2019

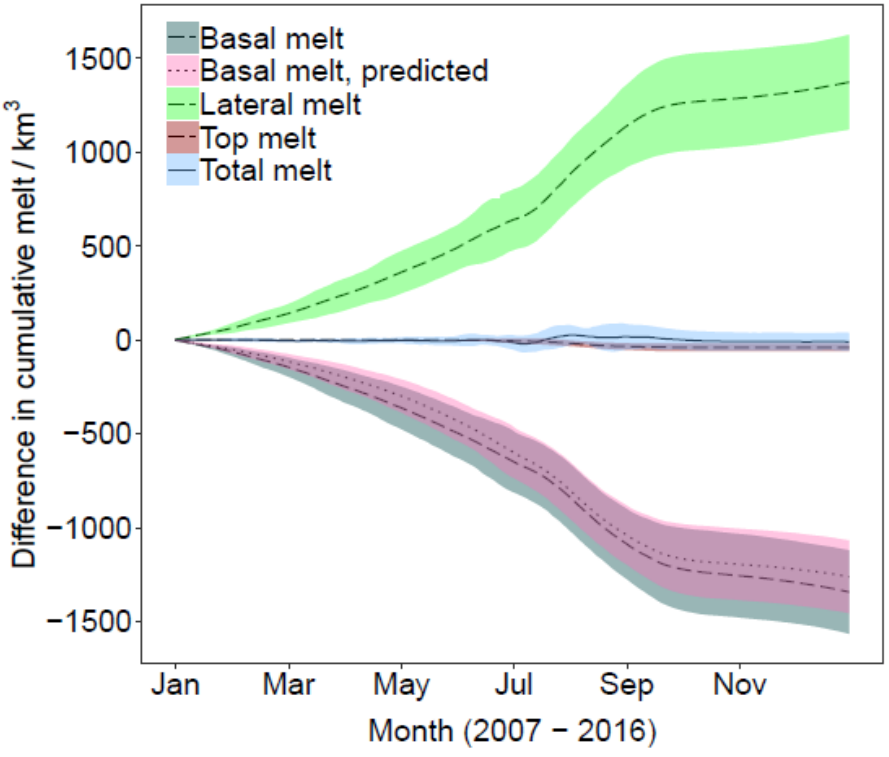

Figure 4: Difference in the cumulative lateral (green ribbon, dashed), basal (grey ribbon, dashed), top (red ribbon, dashed) and total (blue ribbon, solid) melts averaged over 2007 - 2016 between *stan-fsd* relative to *ref*. The ribbon shows, in each case, the region spanned by the mean value plus or minus two times the standard deviation for each simulation. A large increase is observed in the total lateral melt, however this is mostly compensated by a reduction in the basal melt, leading to a negligible change in total melt. A small reduction in top melt can be seen. The predicted difference in basal melt is also shown on the plot (pink ribbon, dotted); this shows the expected change in basal melt accounting only for the reduction in fractional ice area from *ref* to *stan-fsd*.

The Cryosphere Discuss., https://doi.org/10.5194/tc-2019-44
Manuscript under review for journal The Cryosphere
Discussion started: 21 March 2019

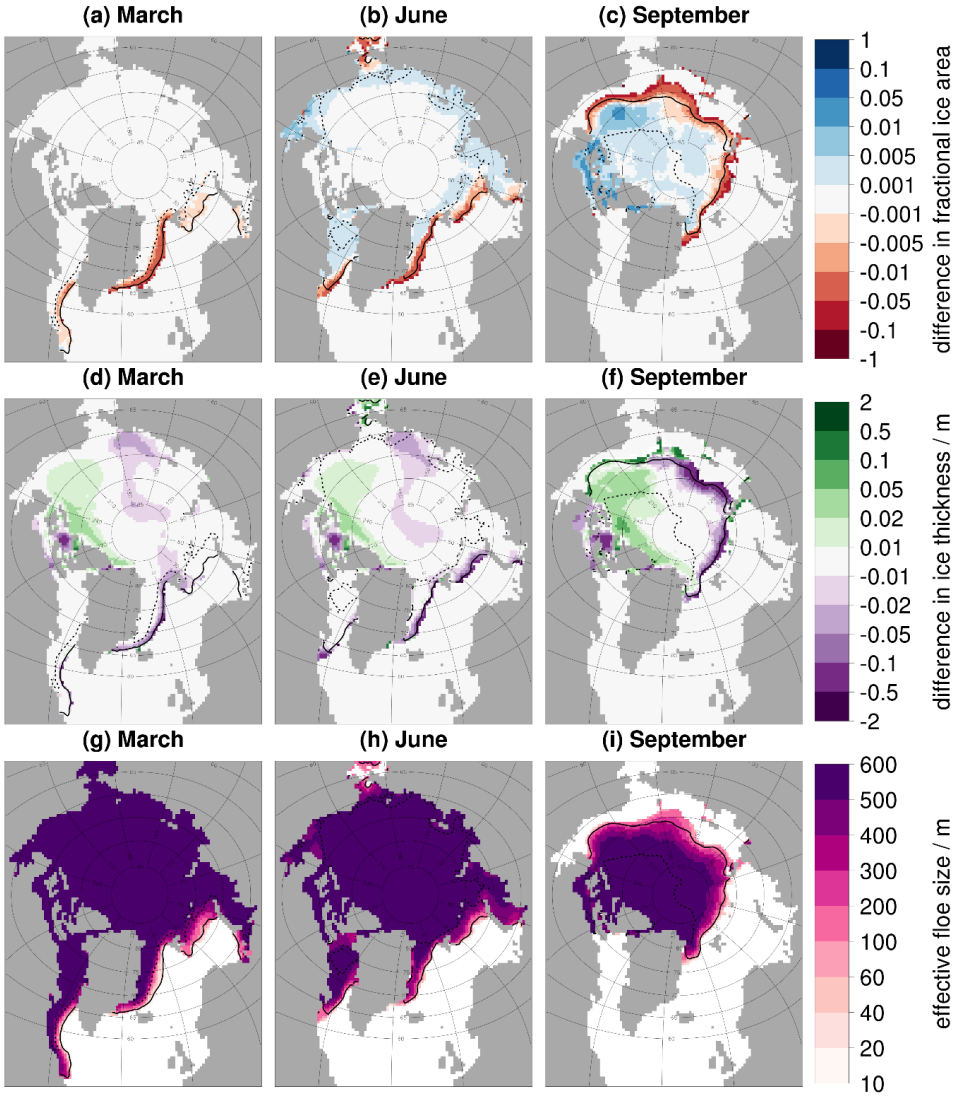

Figure 5: Difference in the fractional ice area (top row, a-c) and ice thickness (middle row, d-f) between *stan-fsd* and *ref* and effective floe size (bottom row, g-i) for *stan-fsd* averaged over 2007 – 2016. Results are presented for March (left column, a, d, g), June (middle column, b, e, h) and September (right column, c, f, i). Values are shown only in locations where the ice area fraction exceeds 5 %. The inner (dashed black) and outer (solid black) extent of the MIZ averaged over the same period is also shown. In general, the plots show an increase in the fractional ice area and ice thickness in the pack ice, but a reduction in the MIZ. This corresponds to the behaviour of the effective floe size, with increases in regions where the effective floe size is above 300 m and reductions where it is below 300 m.

10

The Cryosphere Discuss., https://doi.org/10.5194/tc-2019-44
Manuscript under review for journal The Cryosphere
Discussion started: 21 March 2019

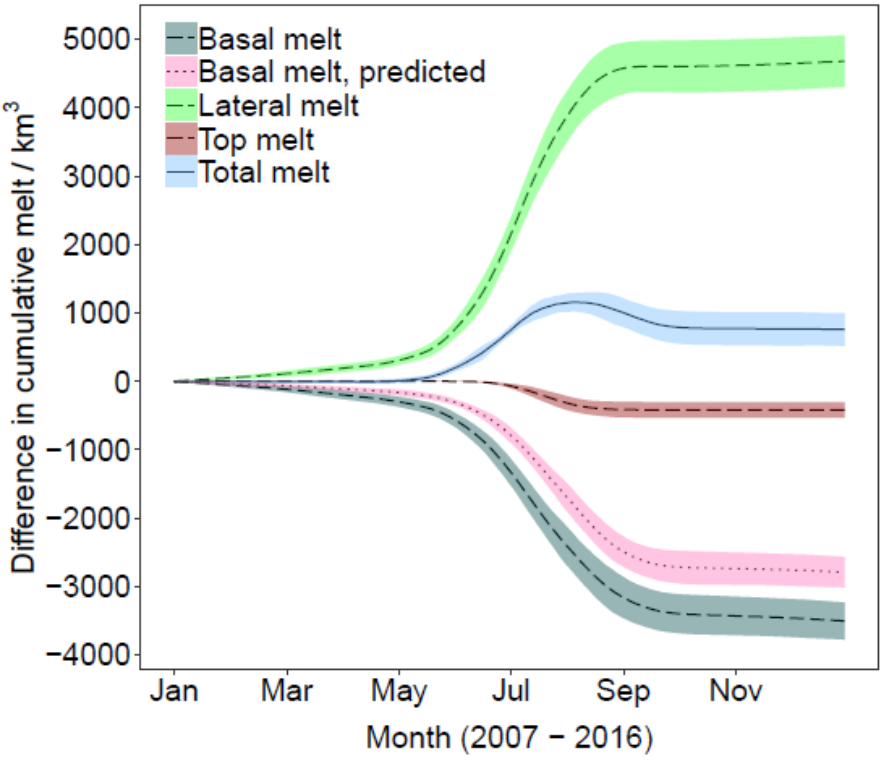

Figure 6: As fig. 4 but the difference between (A) to *stan-fsd* i.e. impact of reducing the exponent from – 2.5 to - 3.5 with the other FSD parameters held at standard values. A large increase in lateral melt is partly compensated by a reduction in basal melt, however this time a large increase is seen in the total melt.

The Cryosphere Discuss., https://doi.org/10.5194/tc-2019-44
Manuscript under review for journal The Cryosphere
Discussion started: 21 March 2019

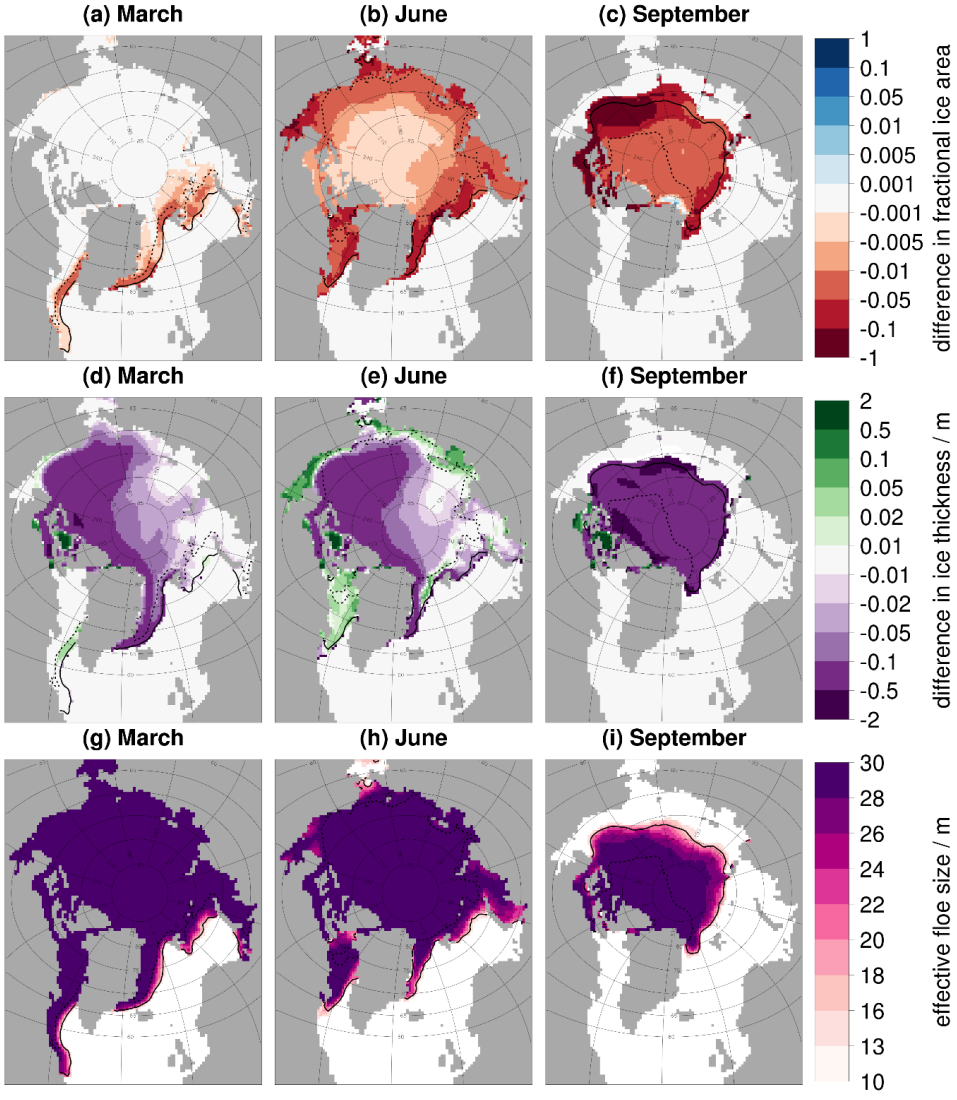

Figure 7: As fig. 5 except now the difference between (A) compared to *stan-fsd* is given i.e. the impact of reducing the exponent from – 2.5 to - 3.5 with the other FSD parameters held at standard values. The effective floe size is reported for the simulation with the more negative exponent. In general, the plots show a reduction in the fractional ice area and ice thickness across the sea ice cover. This corresponds to the behaviour of the effective floe size, with the effective floe size 30 m or below across the sea ice cover.

10

The Cryosphere Discuss., https://doi.org/10.5194/tc-2019-44
Manuscript under review for journal The Cryosphere
Discussion started: 21 March 2019

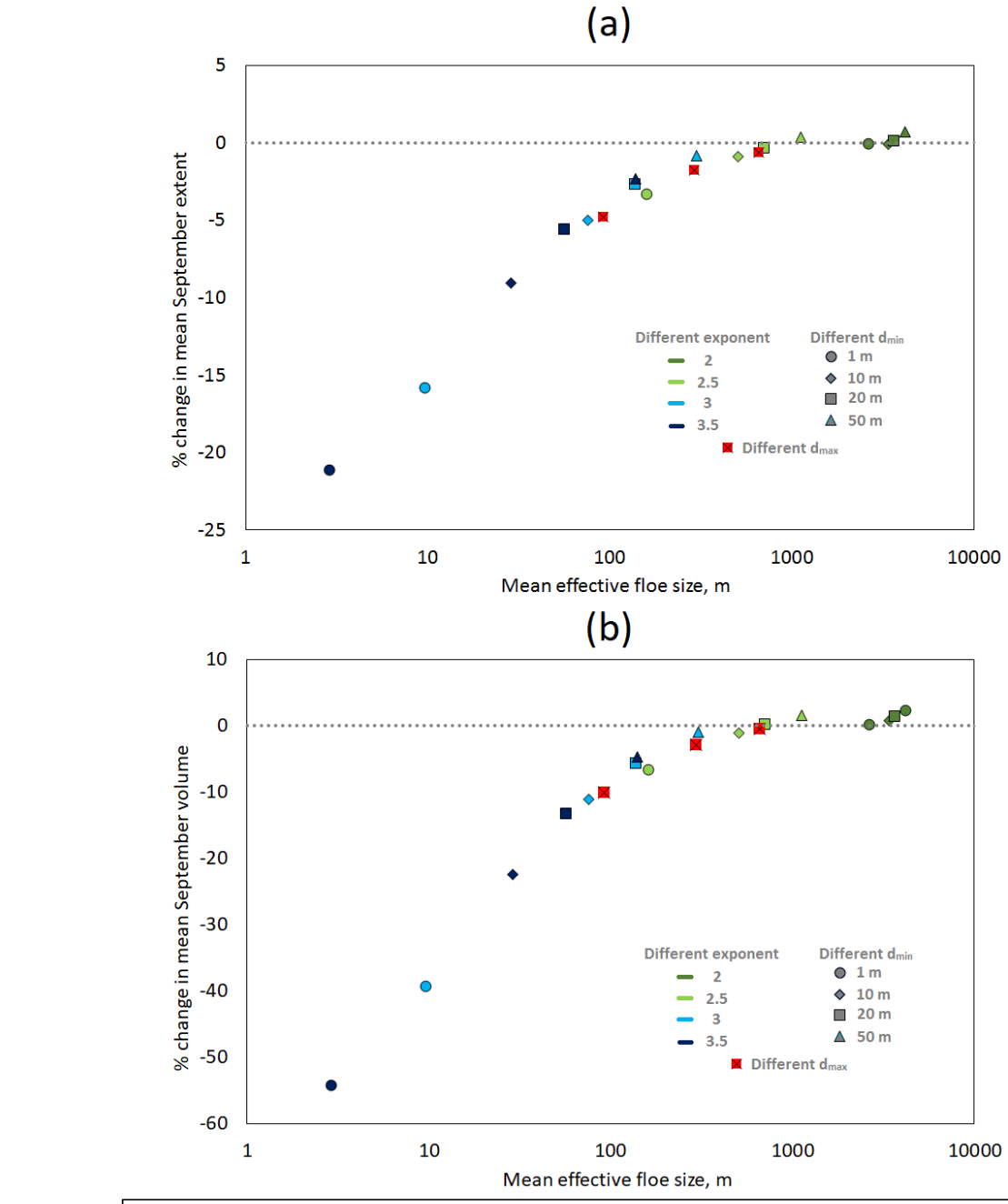

Figure 8: Relative change (%) in mean September sea ice extent (a) and volume (b) from 2007 - 2016 respectively, plotted against mean effective floe size for simulations with different selections of parameters relative to *ref*. The colour of the marker indicates the value of the exponent, the shape indicates value of d_{min}, and the three experiments using standard parameters but different d_{max} (1000 m, 10000 m and 50000 m) are indicated by a crossed red square. The parameters are selected to be representative of a parameter space for the WIPoFSD that has been constrained by observations. Model response ranges from small increases in the sea ice extent and volume to reductions of over 20 and 50 % respectively. The mean effective floe size is shown to be a good predictor of the response of the sea ice extent and volume.

The Cryosphere Discuss., https://doi.org/10.5194/tc-2019-44
Manuscript under review for journal The Cryosphere
Discussion started: 21 March 2019

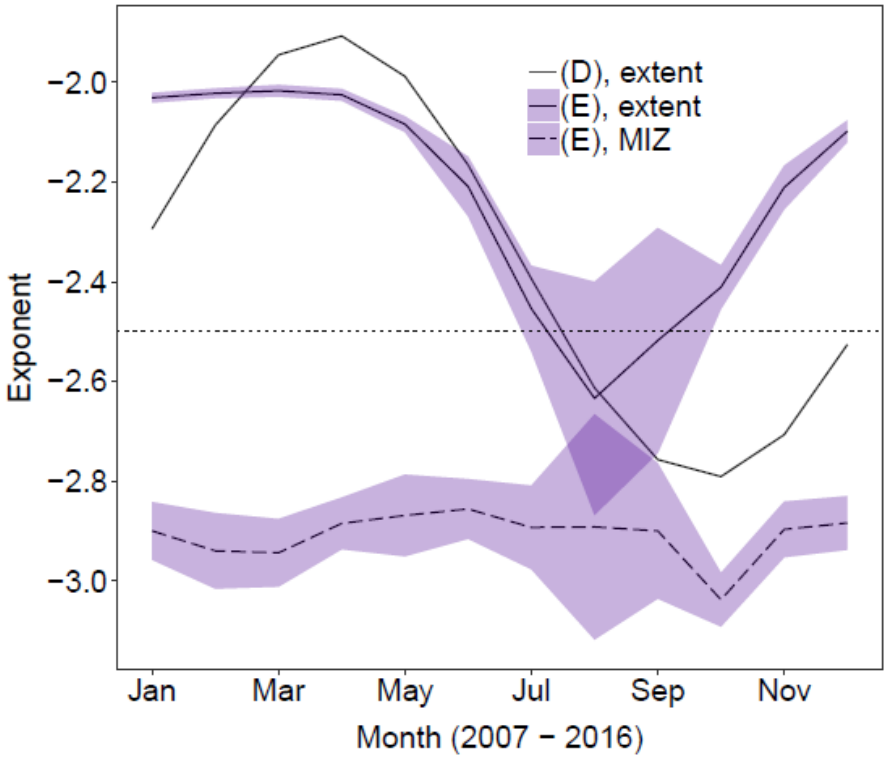

Figure 9: Annual variation in the power law exponent (top) averaged over 2007 – 2016 for two simulations with variable exponents. The plots show results for an exponent which varies depending on time through the year (D, no ribbon) or on the fractional ice area (E, blue ribbon). Results are shown for the total sea ice area (solid) and MIZ only (dashed). The imposed annual oscillation in exponent is identical for all grid cells for (D), hence the MIZ behaviour has not been plotted as it will be identical to the annual oscillation in the exponent across the total sea ice extent. The ribbon shows, in each case, the region spanned by the mean value plus or minus two times the standard deviation for each simulation. Both setups show an annual oscillation in the value of the exponent averaged over the total sea ice extent. For experiment (E), no obvious annual trend in the mean value of the exponent can be seen when averaged over the MIZ, though the interannual variation is at a maximum during the peak melting season between July and September.

The Cryosphere Discuss., https://doi.org/10.5194/tc-2019-44
Manuscript under review for journal The Cryosphere
Discussion started: 21 March 2019

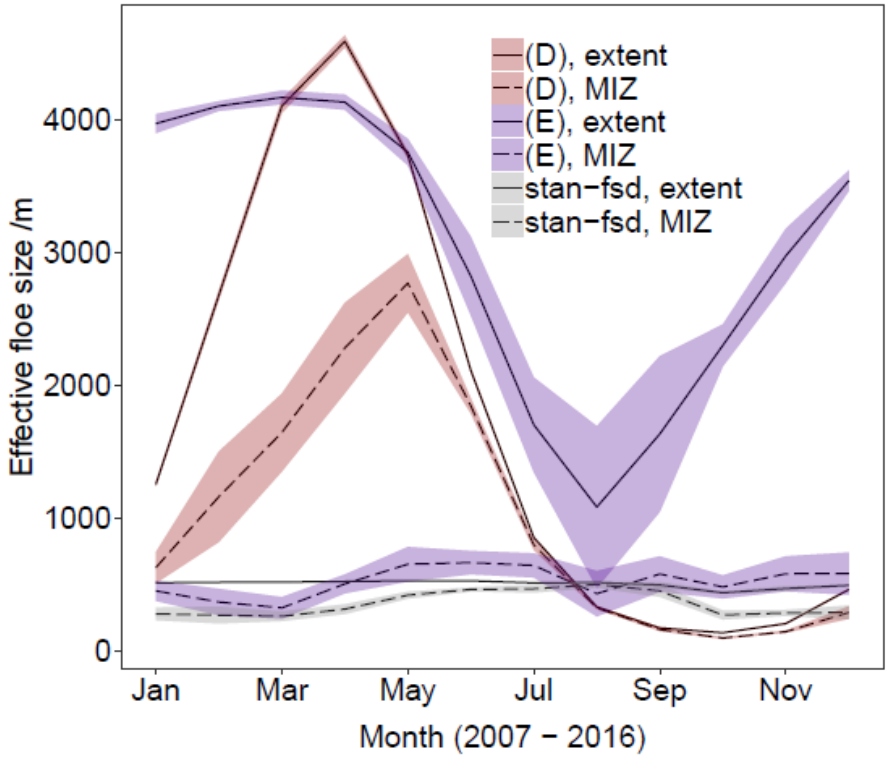

Figure 10: Annual variation in the effective floe size averaged over 2007 – 2016 for two simulations with variable exponents. The plots show the evolution of the effective floe size throughout the year for a simulation with a time-dependent exponent (D, red ribbon) or an ice area fraction-dependent exponent (E, blue ribbon). Also shown is the behaviour of the effective floe size for a simulation with a fixed exponent of -2.5 (*fsd-stan*, grey ribbon). Results are shown for the total sea ice area (solid) and MIZ only (dashed). The ribbon shows, in each case, the region spanned by the mean value plus or minus two times the standard deviation for each simulation. The results show that introducing a variable exponent produces much larger intra-annual variations in effective floe size across the overall sea ice extent than with a fixed exponent. (D) and (E) show an annual oscillation in the value of the effective floe size averaged over the total sea ice extent. Within the MIZ, only experiment (D) continues to show this strong variation in effective floe size; (E) and *fsd-stan* show variations of around an order less. (D) shows the strongest interannual variation between March and May, whereas for (E) it is strongest in the peak melting season between July and August.

The Cryosphere Discuss., https://doi.org/10.5194/tc-2019-44
Manuscript under review for journal The Cryosphere
Discussion started: 21 March 2019

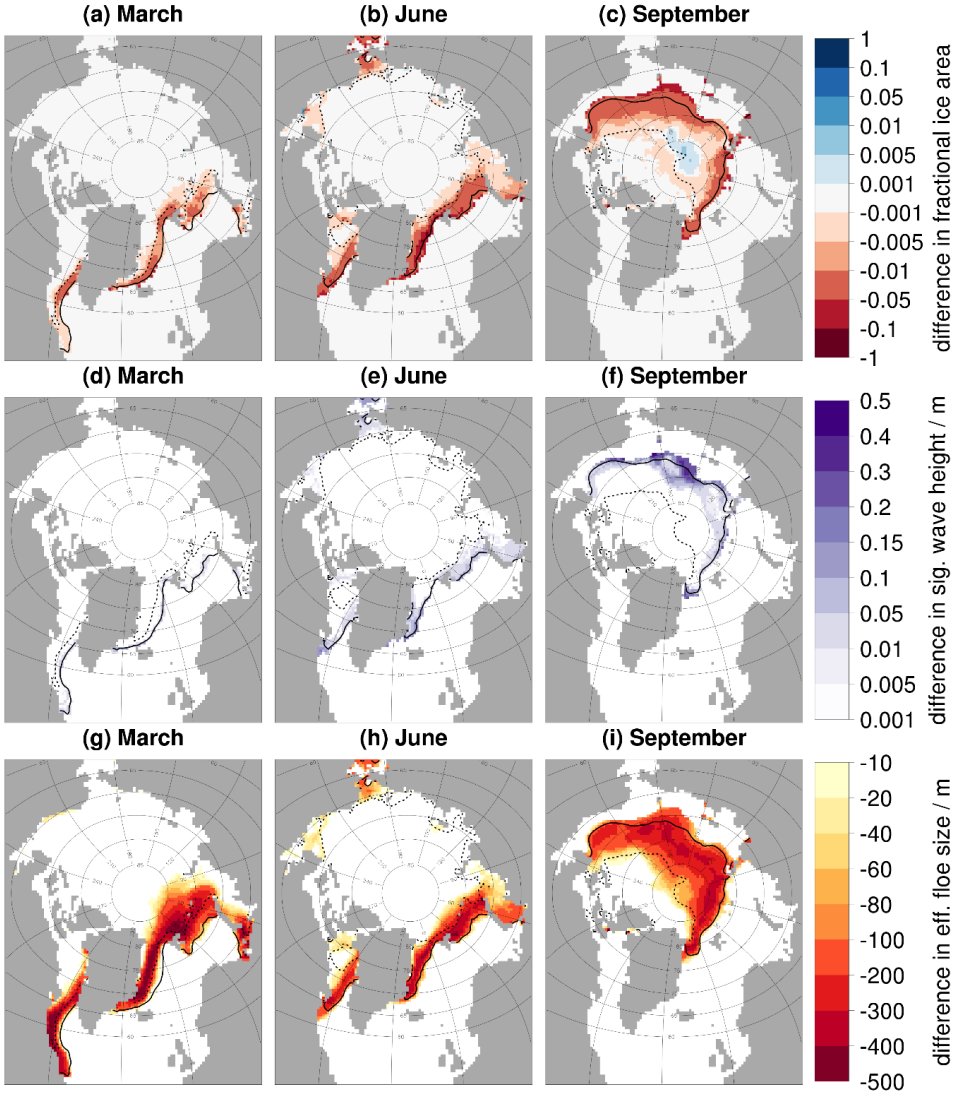

Figure 11: Difference in the fractional ice area (top row, a - c), significant wave height (middle row, d - f) and effective floe size (bottom row, g - i) for (J), with the wave attenuation rate reduced by 90 %, compared to *stan-fsd*, both using standard FSD parameters. Plots show results for March (left column, a, d, g), June (middle column, b, e, h) and September (right column, c, f, i) averaged over 2007 - 2016. Each plot shows the inner (dashed black) and outer (solid black) extent of the MIZ averaged over the same period. Values are shown only in locations where the ice area fraction exceeds 5 %. The plots show that despite very small differences in the significant wave height, the reduced attenuation rate still drives reductions in the effective floe size and in consequence the fractional sea ice area across the MIZ.

The Cryosphere Discuss., https://doi.org/10.5194/tc-2019-44
Manuscript under review for journal The Cryosphere
Discussion started: 21 March 2019

Variable	Description
d_{min}	Fixed minimum floe size within the WIPoFSD model. Standard value of 10 m.
d_{max}	Global maximum floe size within the WIPoFSD model. Standard value of 30000 m.
l_{max}	Local (i.e. grid cell) maximum floe size. Allowed to vary between d_{min} and d_{max}.
α	Power law exponent within the WIPoFSD model. Standard value fixed at -2.5.
l_{eff}	The effective floe size is defined as the floe size of a distribution of identical floes that would produce the same lateral melt rate in a given instant to a distribution of non-uniform floes, when under the same conditions with the same total ice cover. See Eq. (17).
α_{dim}	The dimensional attenuation coefficient, as used in Eq. (6).
P_{crit}	The critical probability that must be exceeded for wave breaking events to occur, as defined in Eq. (7).
T_{rel}	The floe restoring rate, as used in Eq. (12). Set to 10 as default.
α_{shape}	Floe shape parameter to account for the deviation of floes from a perfect circle. Standard value of 0.66 (Rothrock and Thorndike, 1984)
w_{lat}	Lateral melt rate, as calculated within Eq. (2).
m_1	Melt rate parameter, as used in Eq. (2) to calculate the lateral melt rate w_{lat}. Default value of $1.6 \times 10^{-6}\ m\ s^{-1} K^{-m_2}$ (Perovich, 1983)
m_2	Melt rate parameter, as used in Eq. (2) to calculate the lateral melt rate w_{lat}. Default value of 1.36 (Perovich, 1983)

Table 1: Definitions of the parameters relating to the sensitivity studies described in table 2.

The Cryosphere Discuss., https://doi.org/10.5194/tc-2019-44
Manuscript under review for journal The Cryosphere
Discussion started: 21 March 2019

Sensitivity study	Description	Technical details
stan-fsd	CICE-ML with standard FSD	$d_{min} = 10\ m, d_{max} = 30{,}000\ m, \alpha = -2.5$
Ref	CICE-ML with constant floe size	Floe size of 300 m for all floes
(A)	Low exponent	$d_{min} = 10\ m, d_{max} = 30{,}000\ m, \alpha = -3.5$
(B)	Minimum l_{eff}	$d_{min} = 1\ m, d_{max} = 30{,}000\ m, \alpha = -3.5$ This is the selection of FSD parameters that produces the lowest average l_{eff}
(C)	Maximum l_{eff}	$d_{min} = 50\ m, d_{max} = 30{,}000\ m, \alpha = -2$ This is the selection of FSD parameters that produces the highest average l_{eff}
(D)	Exponent evolves over a fixed annual cycle	An annual cycle, as described by Eq. (19), is imposed on the exponent based on the observations of Stern et al. (2018 a). The exponent does not vary spatially.
(E)	Exponent as a function of local ice concentration	The exponent becomes a function of the local sea ice concentration (i.e. fractional sea ice area) according to Eq. (18).
(F)	Waves no longer break-up floes	The waves-in-ice module operates normally, however Eq. (11) is no longer applied after a floe break-up event is identified.
(G)	No lateral melt feedback on floe size	The model operates normally, however l_{max} is no longer reduced based on the amount of lateral melt i.e. Eq. (9) is removed from the model.
(H)	Big waves	The significant wave heights read into the model from ERA-interim data at ice free locations is increased by a factor of 10.
(I)	Weak ice	P_{crit} is reduced by a factor of 10.
(J)	Weaker attenuation of waves	α_{dim} is reduced by a factor of 10.
(K)	Reduced floe growth rates	T_{rel} is increased from 10 to 365.
(L)	Less circular floes	α_{shape} is reduced from 0.66 to 0.44.
(M)	Perfectly circular floes	α_{shape} is increased from 0.66 to 0.79. This is the approximate value of this parameter for a perfect circle.
(N)	Reduced lateral melt rate	The parameters m_1 and m_2 are reduced by 10 % each to $1.44 \times 10^{-6}\ m\ s^{-1} K^{-m_2}$ and 1.22 respectively.
(O)	Increased lateral melt rate	The parameters m_1 and m_2 are increased by 10 % each to $1.76 \times 10^{-6}\ m\ s^{-1} K^{-m_2}$ and 1.48 respectively.
(P)	Shallow mixed layer	The minimum mixed layer depth is reduced from 10 m to 7 m.
(Q)	Deep mixed layer	The minimum mixed layer depth is increased from 10 m to 20 m.

Table 2: The details of the sensitivity studies to explore the behaviour of the CICE-ML-WIPoFSD model. Parameters discussed here defined in table 1.

The Cryosphere Discuss., https://doi.org/10.5194/tc-2019-44
Manuscript under review for journal The Cryosphere
Discussion started: 21 March 2019

Sensitivity study	Description	Metrics (reported as mean September value between 2007 – 2016, parentheses give change from reference)								
		Area metrics / 10^6 km^2		Volume / 10^3 km^3		Mean MIZ l_{eff} / m	Mean MIZ ice perimeter m^{-1}	Annual cumulative melt by end of September / 10^3 km^3			
		Extent	MIZ	Total	MIZ			Top	Basal	Lateral	Total
stan-fsd	CICE-ML with standard FSD	4.70 (0)	2.54 (0)	7.72 (0)	2.07 (0)	453.9	0.0059	5.21 (0)	14.58 (0)	2.43 (0)	22.22 (0)
ref	CICE-ML with constant floe size	4.74 (0.04)	2.61 (0.06)	7.81 (0.09)	2.12 (0.05)	300	0.0068	5.25 (0.04)	15.79 (1.22)	1.17 (-1.26)	22.21 (-0.01)
(a)	Low exponent	4.31 (-0.39)	2.55 (0.01)	6.06 (-1.67)	1.75 (-0.32)	27.7	0.0724	4.79 (-0.42)	11.19 (3.39)	7.03 (-4.60)	23.01 (0.79)
(b)	Minimum l_{eff}	3.76 (-0.96)	2.75 (0.21)	3.56 (-4.16)	1.18 (-0.90)	2.7	0.6850	3.60 (-1.60)	4.34 (-10.23)	16.56 (14.13)	24.50 (2.28)
(c)	Maximum l_{eff}	4.77 (0.07)	2.58 (0.04)	7.98 (0.26)	2.14 (0.07)	3656.3	0.0019	5.27 (0.06)	15.54 (0.96)	1.30 (-1.13)	22.11 (-0.11)
(d)	Exponent evolves over fixed annual cycle	4.69 (-0.01)	2.53 (-0.01)	7.70 (-0.02)	2.06 (-0.01)	162.9	0.0135	5.23 (0.02)	14.68 (0.11)	2.31 (-0.12)	22.22 (0.00)
(e)	Exponent a function of ice concentration	4.55 (-0.15)	2.39 (-0.15)	7.34 (-0.38)	1.85 (-0.22)	580.6	0.0155	5.13 (-0.07)	13.46 (-1.11)	3.75 (1.32)	22.34 (0.12)
(f)	Waves no longer break-up floes	4.78 (0.08)	2.62 (0.08)	7.93 (0.21)	2.15 (0.08)	531.8	0.0038	5.27 (0.06)	15.95 (1.37)	0.93 (-1.50)	22.15 (-0.07)
(g)	No lateral melt feedback on floe size	4.70 (0.01)	2.55 (0.01)	7.75 (0.03)	2.08 (0.01)	465.3	0.0057	5.21 (0.01)	14.69 (0.12)	2.30 (-0.13)	22.20 (-0.02)
(h)	Big waves	4.60 (-0.10)	2.44 (-0.10)	7.47 (-0.26)	1.94 (-0.14)	299.8	0.0178	5.16 (-0.05)	13.62 (-0.96)	3.53 (1.10)	22.31 (0.09)
(i)	Weak ice	4.66 (-0.04)	2.51 (-0.04)	7.65 (-0.08)	2.03 (-0.04)	412.4	0.0080	5.19 (-0.02)	14.26 (-0.32)	2.79 (0.36)	22.24 (0.02)
(j)	Weaker attenuation of waves	4.57 (-0.17)	2.42 (-0.12)	7.40 (-0.33)	1.90 (-0.18)	236.6	0.0276	5.15 (-0.05)	13.42 (-1.16)	3.76 (1.34)	22.33 (0.11)
(k)	Reduced floe growth rates	4.68 (-0.02)	2.54 (0.00)	7.67 (-0.05)	2.06 (-0.01)	372.9	0.0084	5.18 (-0.03)	14.40 (-0.18)	2.67 (0.24)	22.25 (0.03)
(l)	Less circular floes	4.64 (-0.05)	2.50 (-0.04)	7.56 (-0.16)	2.01 (-0.06)	442.2	0.0061	5.17 (-0.03)	14.04 (-0.53)	3.05 (0.63)	22.26 (0.04)
(m)	Perfectly circular floes	4.72 (0.02)	2.56 (0.02)	7.79 (0.07)	2.11 (0.03)	459.1	0.0058	5.22 (0.02)	14.92 (0.34)	2.05 (-0.38)	22.19 (-0.03)
(n)	Reduced lateral melt rate	4.71 (0.01)	2.56 (0.01)	7.74 (0.02)	2.08 (0.01)	456.3	0.0058	5.22 (0.01)	14.77 (0.19)	2.23 (-0.20)	22.21 (-0.01)
(o)	Increased lateral melt rate	4.69 (-0.01)	2.53 (-0.01)	7.70 (-0.02)	2.06 (-0.01)	451.5	0.0060	5.20 (-0.01)	14.41 (-0.17)	2.61 (0.18)	22.22 (0.00)
(p)	Shallow mixed layer	4.70 (0.01)	2.57 (0.03)	7.84 (0.12)	2.14 (0.07)	447.4	0.0056	5.19 (-0.02)	14.56 (-0.01)	2.46 (0.03)	22.21 (-0.01)
(q)	Deep mixed layer	4.64 (-0.06)	2.65 (0.10)	7.62 (-0.11)	2.34 (0.27)	473.6	0.0060	5.26 (0.05)	14.57 (-0.01)	2.34 (-0.08)	22.17 (-0.05)

Table 3: A summary of the metrics for each of the sensitivity studies described in table 2. Metrics are reported for sea ice extent, MIZ extent, total sea ice volume, MIZ volume, mean effective floe size within the MIZ, mean sea ice perimeter per m^2 of ocean area within the MIZ, and cumulative melt top, basal, lateral and total melt. All metrics are reported for September, except the cumulative melt which is reported for all months up to and including September and given as an average between 2007 – 2016. The values in red within the parentheses give the change from *stan-fsd*. Cells highlighted in yellow and orange deviate by one and two standard deviation(s) respectively from the *stan-fsd* mean value (the standard deviation is calculated from the set of 10 annual values for each metric).